HHS Public Access

Author manuscript

Dev Biol. Author manuscript; available in PMC 2023 November 26.

Published in final edited form as:

Dev Biol. 2022 August ; 488: 131–150. doi:10.1016/j.ydbio.2022.05.012.

An enhancer located in a *Pde6c* intron drives transient expression in the cone photoreceptors of developing mouse and human retinas

Vismaya S. Bachu[1,2], **Sangeetha Kandoi**[3,4], **Ko Uoon Park**[1], **Michael L. Kaufman**[1], **Michael Schwanke**[1], **Deepak A. Lamba**[3,4], **Joseph A. Brzezinski IV**[1,5]

[1]Department of Ophthalmology, University of Colorado Anschutz Medical Campus. Aurora, CO.

[2]Johns Hopkins University School of Medicine. Baltimore, MD.

[3]Department of Ophthalmology, University of California San Francisco. San Francisco, CA.

[4]Eli and Edythe Broad Center of Regeneration Medicine and Stem Cell Research, University of California San Francisco. San Francisco, CA.

Abstract

How cone photoreceptors are formed during retinal development is only partially known. This is in part because we do not fully understand the gene regulatory network responsible for cone genesis. We reasoned that cis-regulatory elements (enhancers) active in nascent cones would be regulated by the same upstream network that controls cone formation. To dissect this network, we searched for enhancers active in developing cones. By electroporating enhancer-driven fluorescent reporter plasmids, we observed that a sequence within an intron of the cone-specific *Pde6c* gene acted as an enhancer in developing mouse cones. Similar fluorescent reporter plasmids were used to generate stable transgenic human induced pluripotent stem cells that were then grown into three-dimensional human retinal organoids. These organoids contained fluorescently labeled cones, demonstrating that the *Pde6c* enhancer was also active in human cones. We observed that enhancer activity was transient and labeled a minor population of developing rod photoreceptors in both mouse and human systems. This cone-enriched pattern argues that the *Pde6c* enhancer is activated in cells poised between rod and cone fates. Additionally, it suggests that the *Pde6c* enhancer is activated by the same regulatory network that selects or stabilizes cone fate choice. To further understand this regulatory network, we identified essential enhancer sequence regions through a series of mutagenesis experiments. This suggested that that the *Pde6c* enhancer was regulated by transcription factor binding at five or more locations. Binding site predictions implicated transcription factor families known to control photoreceptor formation and families not previously associated with cone development. These results provide a framework for deciphering the gene regulatory network that controls cone genesis in both human and mouse systems. Our

[5]Author for correspondence. 12800 E. 19th Avenue, RC-1 North 5104, Aurora, CO 80045. USA. 303-724-6959. joseph.brzezinski@cuanschutz.edu.

new transgenic human stem cell lines provide a tool for determining which cone developmental mechanisms are shared and distinct between mice and humans.

Graphical Abstract

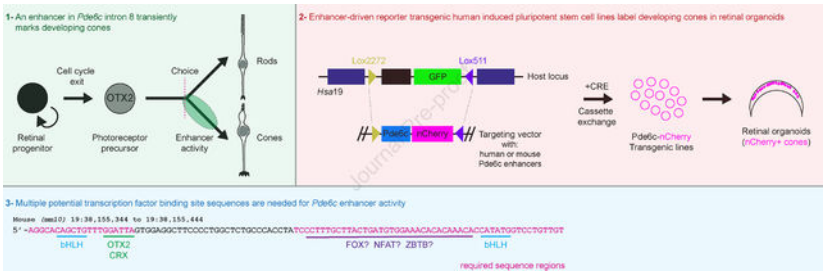

Keywords

Enhancer; Pde6c; cone photoreceptor; retina; iPSC; retinal organoid; development

Introduction

Light stimuli are detected by the rod and cone photoreceptors of the retina. Rods mediate dim light detection while cones are responsible for high-acuity and color vision. In most mammals, including mice and humans, the number of rods in the retina is far greater than cones. In mice, cones are roughly uniformly distributed across the retina and are outnumbered by rods 35-fold (Jeon et al., 1998). The cones of the human retina are non-uniformly distributed. Human cones are more concentrated in the macula, which greatly improves visual acuity in this small region of the retina. Nighttime vision is supported by the much larger surrounding rod-rich retinal tissue. Both rod and cone photoreceptors must last throughout the life of an organism because no regeneration occurs if these cells are lost to injury or disease in adult mammals. The success of regenerative approaches designed to restore vision in blinding diseases is likely to require a deep understanding of the mechanisms of photoreceptor development.

Photoreceptor development is a multistep process. Rods and cones derive from a pool of multipotent retinal progenitor cells. Cell fate decisions made by these progenitors are stochastic, yet correlate with the timing of permanent cell cycle exit (*i.e.*, their “birthdate”) (Bassett and Wallace, 2012; Boije et al., 2014; Brzezinski and Reh, 2015; Cepko, 2014; Xiang, 2013). Experiments correlating cell cycle exit with photoreceptor fate in rodents and primates show that cones are born before rods, though there is considerable overlap (Carter-Dawson and LaVail, 1979; La Vail et al., 1991). In mice, cones are born starting around embryonic day (E) 11.5, peak at E14.5, and are largely finished by birth (Carter-Dawson and LaVail, 1979). Rods are born broadly throughout retinal development (E13.5 to postnatal day (P) 7), but the majority are generated postnatally (Carter-Dawson and LaVail, 1979). Gene expression studies show that human photoreceptor development follows the same cone before rod pattern (Hoshino et al., 2017; Lu et al., 2020). Human developmental studies have been augmented by the creation of three-dimensional (3D) retinal organoid tissue systems

that are derived from unlimited embryonic or induced pluripotent stem cell (iPSC) sources. These human retinal organoids closely mimic human gestational timing, generating cones before rods (Collin et al., 2019; Cowan et al., 2020; Hoshino et al., 2019; Kim et al., 2019; Nakano et al., 2012; Sridhar et al., 2020; Welby et al., 2017; Zhong et al., 2014). In mice and humans, it is thought that a large fraction of progenitors exiting the cell cycle become rod and cone competent photoreceptor precursors (Brzezinski and Reh, 2015; Swaroop et al., 2010). These photoreceptor precursors then decide between rod and cone identities. Cones are further specialized based on which wavelength sensitive opsin (S-short, M-medium, L-long) they express. Human cones form three subtypes defined by unique opsin expression (S, M, and L). In contrast, most mouse cones co-express S and M-opsin in opposing dorsal-ventral gradients (Applebury et al., 2000; Baden et al., 2013; Eldred et al., 2020; Haverkamp et al., 2005; Nadal-Nicolas et al., 2020). After fate is decided, photoreceptors continue to differentiate and acquire their mature gene expression patterns, morphology, and function.

Photoreceptor development is regulated by transcription factors. The homeodomain transcription factor *Otx2* is expressed by a large subset of retinal progenitor cells as they exit the cell cycle (Muranishi et al., 2011). OTX2 is made by photoreceptor precursors and remains expressed in mature rods and cones (Fossat et al., 2007; Koike et al., 2007; Nishida et al., 2003). When *Otx2* is removed from the retina, photoreceptors are not formed (Ghinia Tegla et al., 2020; Nishida et al., 2003; Sato et al., 2007; Yamamoto et al., 2020). OTX2 activates its paralog, *Crx*, in photoreceptor precursors and its expression is maintained into adulthood (Chen et al., 1997; Furukawa et al., 1997; Nishida et al., 2003). Unlike *Otx2* mutants, mice lacking *Crx* still generate photoreceptors (Furukawa et al., 1999). However, these mutant rods and cones do not mature normally and eventually undergo cell death (Furukawa et al., 1999). Developing rods express the MAF transcription factor *Nrl* and the nuclear receptor *Nr2e3* (Akimoto et al., 2006; Brightman et al., 2016; Bumsted O'Brien et al., 2004; Mears et al., 2001; Peng et al., 2005). *Nrl* mutants lack rods and have excess S-cones, indicating that this transcription factor selects or stabilizes rod fate choice in photoreceptor precursors (Cuevas et al., 2021; Kallman et al., 2020; Mears et al., 2001). Mutating *Nr2e3* results in ectopic cone marker (*e.g.*, S-opsin) expression in rods (Chen et al., 2005; Corbo and Cepko, 2005). The nuclear receptors *Rxrg* (NR2B3) and *Thrb* (NR1A2) are made by developing cones (Mori et al., 2001; Ng et al., 2001; Roberts et al., 2005; Sjoberg et al., 1992). Deleting these genes does not prevent cone formation, but instead alters opsin expression. *Thrb* mutants lack M-opsin while *Thrb* and *Rxrg* mutants each have excess S-opsin expression (Eldred et al., 2018; Ng et al., 2001; Roberts et al., 2005; Roberts et al., 2006). These data argue that *Thrb* and *Rxrg* act downstream of the decision to become a cone, instead influencing subtype identity. Other more broadly expressed transcription factors that precede *Thrb* and *Rxrg* have modest cone photoreceptor deficits when mutated. This includes the homeodomain transcription factors *Onecut1* and *Pou2f* and the basic helix-loop-helix (bHLH) factor *Neurod1* (Emerson et al., 2013; Javed et al., 2020; Liu et al., 2008; Sapkota et al., 2014). How these and other transcription factors function in a network to determine cone fate choice is unclear.

Transcription factors regulate gene expression by binding non-coding DNA elements known as enhancers. Deciphering how enhancers function reveals components of the upstream

regulatory network that controls developmental events. We hypothesized that enhancers active early within developing cones will be regulated by the transcription factor network that controls cone fate choice. Enhancers are often located in genomic regions that are accessible to nucleases. Therefore, we searched for regions of accessible chromatin around cone-specific genes using accessibility datasets derived from developing mouse retinas (Aldiri et al., 2017). We identified accessible regions (*i.e.*, potential cone enhancers) within the *Pde6c* gene, a phosphodiesterase that is specific to cone photoreceptors (Lamb, 2020). Enhancer activity was screened by electroporating plasmid-based fluorescent reporter constructs into embryonic mouse retinal explants. We observed that a sequence element within intron 8 of *Pde6c* drove transient expression in developing mouse cones. This mouse element and the homologous human sequence were used to make transgenic human iPSC reporter lines. When these lines were grown into human retinal organoids, both the mouse and human transgenes transiently labeled developing cones. In both mouse explant and human organoid systems, a small number of rods were labeled, suggesting that the *Pde6c* intron 8 sequence is an enhancer that marks cells poised between rod and cone identity. Mutagenesis of the mouse enhancer sequence revealed several regions that were required for its activity. Binding site predictions made within the required sequences implicated suspected (OTX2/CRX and bHLH) and unexpected (FOX, NFAT, and ZBTB) transcription factors in *Pde6c* enhancer regulation. Which transcription factors regulate the enhancer, whether they decide cone fate, and how they are utilized differently in human retinas remains to be determined.

Results

An intronic sequence in Pde6c drives expression in developing mouse photoreceptors

The mechanisms that control cone photoreceptor fate choice are poorly understood. We reasoned that identifying and decoding DNA sequences that act as early cone enhancers would reveal the gene regulatory network responsible for cone genesis. To identify early cone enhancers, we searched for cone-specific genes that were expressed during embryonic development. We previously identified several embryonically expressed genes that were activated after pan-photoreceptor genes (*Otx2*, *Prdm1*, and *Crx*), but with similar timing to known cone markers *Rxrg* and *Thrb* (Kaufman et al., 2019; Mori et al., 2001; Ng et al., 2001; Roberts et al., 2005; Sjoberg et al., 1992). We pursued one well-known cone-specific candidate from this list- *Pde6c* (*Phosphodiesterase 6c*) (Kaufman et al., 2019). Although the *Pde6c* gene acts in phototransduction (Lamb, 2020), we hypothesized that the transcription factors that activate its expression embryonically also regulate cone development.

Enhancers are located in regions of nuclease (or transposase) accessible chromatin.
We utilized assay for transposase-accessible chromatin with high throughput sequencing (ATAC-seq) datasets (Aldiri et al., 2017) to identify open chromatin regions within the developing mouse retina. These datasets were generated from whole retinal tissue from E14.5 to adult stages (Fig 1A, S1) (Aldiri et al., 2017). We identified accessible chromatin regions within and adjacent to the *Pde6c* gene (Fig 1A, S1). These included ATAC-seq peaks within introns 1 and 8 (Fig 1, S1). Two peaks near the *Pde6c* transcription start site were not considered further because promoter regions are frequently accessible regardless

of expression (Fig 1, S1) (Fenouil et al., 2012; Wu et al., 2018). The peak in intron 1 was weak at early developmental stages and became prominent in the adult retina (Fig 1A, S1). In contrast, the peak in intron 8 was strongest during development and weak in the mature retina (Fig 1A, S1). The peak from intron 8 had little accessibility in adult rod- or cone-specific ATAC-seq datasets (Murphy et al., 2019) (Fig S2). However, the intron 1 peak was more prominent in mature cones than in rods (Fig S2). Together, these data show that the intron 8 peak has early and transient accessibility. This is consistent with a role for the intron 8 sequence in developing cones.

To determine if the ATAC-seq peaks within introns 1 and 8 act as enhancers, we used an *ex vivo* retinal electroporation assay to screen for their activity (Kaufman et al., 2021; Mills et al., 2017; Wilken et al., 2015) (Fig 1B). For this, we cloned the intron 1 peak sequence (677 base pairs [bp]) and the intron 8 sequence (569bp) upstream of a minimal TATA promoter and a nuclear-localized (n) GFP cassette (pMin-nGFP) (Kaufman et al., 2021; Wilken et al., 2015) (Fig 1B, Supplemental Table 1). As a positive control for electroporation, we used a plasmid in which the red fluorescent protein (RFP) nCherry is driven by the ubiquitous *EF1a* promoter (EF1a-nCherry) (Wilken et al., 2015) (Fig 1B). As a negative control, we utilized GFP plasmids that lacked any enhancer sequences (TATA-only). One nGFP plasmid and the control nCherry plasmid were co-electroporated into mouse E13.5 retinal explants and cultured for two days *in vitro* (DIV) (Fig 1B). The explants were fixed, cryopreserved, sectioned, and subjected to immunohistochemistry for RFP (Cherry) to detect electroporated cells, GFP to detect enhancer activity, and for OTX2 to mark developing photoreceptors (Fossat et al., 2007; Koike et al., 2007; Nishida et al., 2003) (Fig 1C–E”). In the TATA-only control, there were rarely any GFP+ cells, despite abundant Cherry+ electroporated cells (Fig 1C–C”). This showed that there was little endogenous activity from the minimal promoter plasmid, as observed previously (Kaufman et al., 2021; Mills et al., 2017). Similarly, we did not observe any activity from the intron 1 sequence in retinal explants despite robust electroporation (Fig 1D–D”). In contrast, GFP expression was observed in retinas electroporated with the intron 8 sequence (Fig 1E–E”). While the Cherry+ cell pattern was spread throughout the retina, the GFP pattern was highly localized to the outer aspect of the retina where newly formed photoreceptors reside. Correspondingly, nearly every GFP+ cell co-expressed the photoreceptor marker OTX2 (Fig 1E–E”).

We further focused on the *Pde6c* intron 8 sequence, dissecting it into a series of three smaller sub-elements called Pde6c-1, 2, and 3 for simplicity (Fig 2, Supplemental Table 1). Each of these sequences was cloned into the pMin-nGFP vector and electroporated into E13.5 retinal explants along with EF1a-nCherry. After 2 DIV, we conducted immunohistochemistry for GFP, RFP (Cherry), and OTX2 (Fig 2A–C”). All three sub-elements of the intron 8 sequence showed a similar pattern of GFP expression, with a modest number of nuclei present in the outer-most aspect of the retina (Fig 2A–C”). GFP+ cells nearly completely overlapped with OTX2 (means = 97, 99, and 96%), which contrasted with control Cherry+ electroporated cells at a mean of 31% (± 8% standard deviation [SD]) (Fig 2A–C”, 2G). Compared to Cherry control, intron 8, Pde6c-1, Pde6c-2, and Pde6c-3 GFP+ cells were significantly enriched for OTX2 overlap (Kruskal-Wallis with Dunn’s multiple comparisons tests, $P < 0.0001$ for each) (Fig 2G). The percentage of GFP+ cells co-expressing OTX2 was not significantly different between these four conditions (means =

95, 97, 99, and 96%) (Fig 2G), suggesting that each is capable of driving the same spatial pattern. We further dissected the smallest common sequence, Pde6c-3, into 4 sub-elements (A-D) (Fig 2H, Supplemental Table 1). These were electroporated into E13.5 explants and examined as above (Fig 2D–F"). Elements Pde6c-3A and Pde6c-3B had GFP localized to the outer-most aspect of the retina, similar to the parental intron 8 element (Fig 2D–D" and data not shown). GFP+ cells from Pde6c-3A and Pde6c-3B elements had nearly complete overlap with OTX2 (means = 99 and 95%) (Fig 2D–D", 2G). This overlap was not significantly different from any of the larger constructs (Fig 2G–H). In contrast, the smaller Pde6c-3C and Pde6c-3D elements lacked GFP activity despite the abundance of Cherry+ electroporated cells (Fig 2E–F"). From this, the smallest sequence that recapitulated the parental intron 8 pattern was the 101bp *Pde6c-3B* sequence (Fig 2H).

The Pde6c intron 8 enhancer drives expression in developing mouse cones

Pde6c intron 8 and its active sub-elements were expressed by OTX2+ cells, suggesting that these constructs mark developing photoreceptors. At embryonic times, OTX2 marks rods, cones, and cells that are still deciding between multiple fates (Baas et al., 2000; Brzezinski and Reh, 2015; Brzezinski et al., 2013; Emerson et al., 2013; Fossat et al., 2007; Koike et al., 2007; Muranishi et al., 2011; Nishida et al., 2003; Sato et al., 2007). The relatively low number of GFP+ cells seen in electroporations suggested that only a subset of OTX2+ cells were being marked. This is consistent with a cone-restricted pattern of GFP expression. To test this, we stained electroporated retinas for GFP and the cone marker RXRG (Mori et al., 2001; Roberts et al., 2005) (Fig 3). We screened the parental intron 8 element and the five active sub-elements (Fig 2). GFP+ cells frequently co-expressed RXRG in all six enhancer constructs tested (means = 91, 81, 83, 85, 83, and 89%) (Fig 3). Overall, roughly 85% of GFP+ cells co-expressed RXRG (Fig 3G). This overlap was lower than seen with OTX2 (> 95%), suggesting that some of the GFP+ cells are rod photoreceptors or have not yet fully stabilized cone identity. As before, there was no significant difference in the percentage of GFP+ cells that co-expressed RXRG between sub-elements (Kruskal-Wallis with Dunn's multiple comparison test, $P > 0.05$ for each). The parental and minimal Pde6c-3B elements each drive expression in a strongly cone-enriched fashion.

To further demonstrate the cone-specificity of the intron 8 family of elements, we examined retinal explants forced to generate excess cones. For this, we electroporated the enhancer GFP plasmids into E14.5 mouse retinal explants and treated them with the γ-secretase inhibitor DAPT (Kaufman et al., 2019) (Fig S3). We previously showed that this greatly increased the number of cones and cone-specific gene expression by 48 hours of treatment (Kaufman et al., 2019). Electroporated DAPT treated explants were collected after 2 DIV and immunostained for GFP and RXRG. As expected, the DAPT treatment greatly increased the number of RXRG+ cones and the number of GFP+ cells increased in parallel with the number of RXRG+ cells (Fig S3). Nearly all of the GFP+ cells co-expressed RXRG (Fig S3). The increase in GFP+/RXRG+ cells in DAPT treated retinas indicates that the intron 8 element and its derivatives preferentially mark developing cone photoreceptors.

The Pde6c intron 8 enhancer lineage includes cones and a small number of rods

To more fully investigate the cell types that the *Pde6c* intron 8 enhancer marks, we conducted lineage tracing studies. We utilized previously generated plasmid constructs containing a TATA minimal promoter driving GFP along with Cre recombinase linked by a self-cleaving peptide (P2A) sequence (Fig S4) (Goodson et al., 2020b; Kaufman et al., 2021). We cloned the intron 8 sequence upstream of the TATA box minimal promoter in this construct to generate the lineage tracing plasmid. We validated the lineage tracing plasmid by electroporating it into E14.5 explants and culturing them for 2 DIV (Fig S4). As above, immunostaining showed that GFP preferentially marked OTX2+ and RXRG+ cells (Fig S4B–C"). Furthermore, adding DAPT to the cultures strongly increased the number of GFP+ cells, which overwhelmingly expressed the cone marker RXRG (Fig S4D–D"). Lastly, we examined GFP+ cells for co-expression of Cre recombinase. We found that Cre immunostaining overlapped with GFP (Fig S4E–E"'). Taken together, these data indicated that the lineage tracing construct recapitulated the intron 8 expression pattern.

To trace the lineage of intron 8+ cells, we initially attempted to create transgenic mice. We used a linearized version of the lineage tracing plasmid lacking non-essential backbone sequences. Despite multiple rounds of pronuclear injections, we obtained only three potential founders that were all female. These founders either did not breed or failed to transmit the transgene to their progeny. To overcome our failure to generate transgenic mice, we conducted lineage tracing by electroporating plasmids into *ROSA26-lox-stop-lox-tdTomato* (*ROSA-RFP*) (Madisen et al., 2010) mouse retinal explants. As a specificity control, we created a lineage tracing plasmid containing the ubiquitous *EF1a* promoter instead of intron 8. We electroporated retinal explants from E13.5 *ROSA-RFP* mice with either intron 8 or EF1a control lineage tracing plasmids (Fig 4A). Explants were cultured at the air-media interface for 7 DIV and examined by immunohistochemistry for GFP, RFP, and RXRG (Fig 4B–C'). At 7 DIV, we observed numerous RFP+ cells in control electroporations (Fig 4B–B'). The RFP+ cells were diverse in appearance and their morphologies were consistent with progenitor, interneuron, and photoreceptor identities (Fig 4B). A small fraction of these RFP+ cells co-expressed RXRG (Fig 4B'). In contrast, the *Pde6c* lineage tracing resulted in a uniform appearance of RFP+ cells (Fig 4C). Most cells had a photoreceptor morphology and co-expressed RXRG (Fig 4C'). We did not see GFP expression in the *Pde6c* lineage traced explants. These data are consistent with the *Pde6c* intron 8 element driving a transient cone-specific expression pattern. Nonetheless, not all of the RFP+ cells co-expressed RXRG. To determine whether some of the photoreceptors in the *Pde6c* lineage traced explants were rods, we stained for the rod marker NR2E3 (Bumsted O'Brien et al., 2004; Peng et al., 2005). However, NR2E3 staining was not robust after 7 DIV. To overcome this problem, we electroporated E13.5 *ROSA-RFP* retinal explants with *EF1a* or *Pde6c* lineage tracing plasmids and cultured them for 14 DIV. After 14 days, NR2E3 was readily detected (Fig 4, S5). The longer culturing period also had the advantage of allowing undifferentiated cells time to select an identity and become more mature. The chief limitation of the 14 DIV period was that the explants extensively formed rosettes. We immunostained these 14 DIV cultures with antibodies against RXRG (cones), NR2E3 (rods), and OTX2 (photoreceptors dim, bipolars intense) (Fig 4D–I'). As seen at 7 DIV, the *EF1a* lineage at 14 DIV contained numerous RFP+ cells with conspicuous photoreceptor

and interneuron morphologies (Fig 4D, F, H). In contrast, the *Pde6c* lineage had far fewer RFP+ cells, but these nearly always had photoreceptor morphology (Fig 4E, G, I). No GFP+ cells were seen, consistent with transient enhancer activity. A relatively small fraction (19% ± 5% SD) of the *EF1a* lineage traced cells overlapped with RXRG, while the majority (79% ± 9% SD) of RFP+ cells in the *Pde6c* lineage co-expressed RXRG (Fig 4D–E', J). This large difference in the percentage of cells that co-expressed RFP and RXRG was statistically significant (Mann-Whitney test, $P < 0.0001$). The majority (60% ± 8% SD) of RFP+ cells in the *EF1a* lineage tracing condition co-expressed NR2E3, consistent with the high number of rods that make up the mouse retina (Fig 4F–F', K). The *Pde6c* lineage had a significantly (Mann-Whitney test, $P < 0.0001$) lower percentage (21% ± 10% SD) of RFP+ cells that co-expressed NR2E3 (Fig 4G–G', K). This indicates that a modest fraction of cells in the *Pde6c* lineage adopts rod fate. When added together, the mean percentage of RFP+ cells that co-expressed NR2E3 (21%) and RXRG (79%) was essentially 100% in the *Pde6c* condition. However, the variance seen in overlap percentages led us to examine whether RXRG and NR2E3 were co-expressed at 14 DIV (Fig S5). Interestingly, we observed that about 6% of the RXRG+ cells made NR2E3 (Fig S5). Because NR2E3 cells are more abundant than RXRG, a much smaller fraction of the NR2E3+ population co-expressed RXRG (Fig S5). Whether RXRG+/NR2E3+ cells represent rods or cones is unclear. Regardless, the small number of these double-labeled cells cannot account for the 21% of RFP+ cells that co-expressed NR2E3 in the *Pde6c* lineage tracing condition. This argues that at least 15% of the cells in the *Pde6c* lineage are rods. Lastly, we stained for OTX2 to mark all photoreceptors and bipolar cells. The majority (71% ± 7% SD) of RFP+ cells in the *EF1a* lineage co-expressed OTX2 (Fig 4H–H', L). This included dimly labeled photoreceptors and intensely labeled bipolar cells (Fig 4H–H'). This percentage is consistent with the relative abundance of OTX2+ cell types in the mouse retina (Jeon et al., 1998). The RFP+ cells in the *Pde6c* lineage nearly always (96% ± 4% SD) co-expressed OTX2 (Fig 4I'–I', L). This overlap was significantly higher than in the *EF1a* lineage condition (Mann-Whitney test, $P < 0.0001$) (Fig 4L). The double-labeled cells in the *Pde6c* lineage tracing typically had a dim OTX2 staining pattern that was consistent with photoreceptor identity (Fig 4I–I'). A small fraction of RFP+ cells (~4%) in the Pde6c lineage did not co-express OTX2 (Fig 4L). It is unclear whether this indicates that a small population of cells normally activates the *Pde6c* enhancer and goes on to adopt non-OTX2+ cell fates or if a minor amount of non-specific recombination occurs whenever Cre plasmids are electroporated into *ROSA-RFP* explants. In aggregate, these data show that the *EF1a* and *Pde6c* constructs label distinct lineages. The *Pde6c* intron 8 lineage is narrowly restricted to photoreceptors with an approximately four-to-one preference for cones over rods.

The Pde6c intron 8 enhancer drives transient expression in the cones of human retinal organoids

In mice, the *Pde6c* intron 8 enhancer drives transient expression in cones and a small fraction of rods. We next tested whether this enhancer was active in developing human cone photoreceptors. To investigate this, we made transgenic human iPSC lines and differentiated them into 3D retinal organoids. We acquired a genetically modified iPSC line that contained a ubiquitously expressed GFP cassette inserted into the *AAVS1* safe harbor locus on chromosome 19 (AAVS1-copGFP) (Pei et al., 2015) (Fig S6). The GFP insert is flanked by

Lox2272 and Lox511 sites, which allows for cassette exchange with a targeting plasmid in the presence of Cre recombinase (Fig S6). We utilized a cassette exchange strategy to insert the *Pde6c* enhancer into the *AAVS1* locus in these iPSCs. To do this, we built two different targeting constructs to modify the AAVS1-copGFP iPSC line. The first contained the mouse *Pde6c-3B* minimal enhancer sequence (101bp) driving nCherry (Fig S6). The other targeting plasmid contained the human (h) *PDE6C* sequence (715bp) homologous to the mouse intron 8 element driving nCherry (Fig S6, Supplemental Table 1). The AAVS1-copGFP iPSCs were given Cre and either mouse or human targeting vectors to cause cassette exchange (Fig S6). Successful targeting resulted in the loss of GFP expression and puromycin resistance and the acquisition of neomycin resistance (Fig S6). One successfully targeted iPSC clone from each line was used to generate 3D human retinal organoids (Fig 5).

We first examined mouse Pde6c-3B-nCherry transgenic iPSCs (Fig 5A–E”’) to determine whether the enhancer marked developing human cones. At 45 days of culture, human retinal organoids were forming cone photoreceptors, as marked by RXRG and OTX2 co-expression (Fig 5B–B”’). We observed numerous Cherry+ cells in the outer aspect of the retinal organoids, where cones were forming (Fig 5B–B”’). The Cherry+ cells nearly always (99% ± 2% SD) co-expressed OTX2, consistent with a photoreceptor identity (Fig 5B–B”’, 5H). These Cherry+ cells co-expressed RXRG 90% (± 10% SD) of the time, suggesting that most of them were developing cones (Fig 5B–B”’, 5H). At 59 days, we observed a similar pattern (Fig 5C–C”’). Nearly all of the Cherry+ cells were OTX2+ (99% ± 1% SD) or RXRG+ (96% ± 3% SD) (Fig 5C–C”’, 5H). Almost all of the RXRG+/OTX2+ cones were Cherry+ at both 45 (97% ± 3% SD) and 59 (97% ± 2% SD) days of culture. Together, these data indicate that the mouse Pde6c-3B enhancer marks nearly the entire population of developing human cone photoreceptors. Since we found rods in the *Pde6c* lineage in mice, we examined 120-day organoid cultures when rod production is ramping up and cone genesis is nearly complete (Nakano et al., 2012; Sridhar et al., 2020; Zhong et al., 2014) (Fig 5D–E”). At 120 days, we observed RXRG+/OTX2+ cones in the outer side of the organoid (Fig 5D–D”’). Unlike at 45 and 59 days, Cherry expression was weaker and labeled far fewer cells (Fig 5D–E”’). Only a subset of RXRG+/OTX2+ cones still co-expressed Cherry (Fig 5D–D”’). This is consistent with the transient enhancer expression we observed in mice. We also stained the organoids with the rod marker NRL (Akimoto et al., 2006; Mears et al., 2001) (Fig 5E–E”’). We observed that a small number of Cherry+ cells co-expressed NRL, consistent with this enhancer marking a small population of rods (Fig 5E–E”’). In many cases, these Cherry+/NRL+ cells had modest RXRG co-staining (Fig 5E–E”’). This was similar to what we observed in mice (Fig S5), where some cells co-expressed RXRG and NR2E3. Together, these data show that the mouse *Pde6c* minimal enhancer sequence drives transient activity in human cones and in a much smaller population of rods.

Next, we tested whether the human *PDE6C* sequence drove a similar pattern of expression in human organoids (Fig 5F–G). Organoids were examined at 45 and 59 days (Fig 5G–G”’). We observed the same pattern seen with the mouse enhancer at 45 days, with the majority of Cherry+ cells showing OTX2+ (99% ± 1% SD) or RXRG+ (87% ± 8% SD) co-expression. At 59 days, nearly all of the Cherry+ cells co-expressed OTX2 (97% ± 5%) or RXRG (95% ± 5% SD) (Fig 5G’–G”’, I). Almost all of the OTX2+/RXRG+ cones co-expressed Cherry at both 45 (95% ± 4% SD) and 59 (96% ± 4% SD) days. We compared

the percentage of Cherry+ cells that co-expressed OTX2 and RXRG (Fig 5H–I) between mouse and human enhancers using Kruskal-Wallis one-way ANOVA with Dunn's multiple comparisons tests. We did not find significant differences between the percentage overlap with OTX2 or RXRG between the 45- and 59-day time points or between mouse and human enhancers ($P > 0.05$). We also examined these organoids at 120 days of culture and observed few Cherry+ cells (data not shown). This parallels the results with the mouse enhancer line (Fig 5D–E"'). Taken together, these data argue that both the human and the mouse *Pde6c* enhancer sequences drive transient expression in nearly the entire population of developing human cone photoreceptors. While the spatial and temporal patterns between mouse and human enhancers were equivalent, the Cherry fluorescence in the mouse Pde6c-3B line was moderately more intense.

Since the *hPDE6C* sequence behaved similarly to mouse, we examined whether the human enhancer drove expression in developing murine cones. We built a plasmid where hPDE6C drove nCherry and co-electroporated it with a ubiquitously expressed GFP plasmid into E14.5 mouse explants (Fig S7). After 2 DIV, we did not observe any Cherry+ cells in the retina (Fig S7). This suggested that the human enhancer does not have activity in the mouse retina. We then repeated the electroporation, but treated the retinal explants with the γ-secretase inhibitor DAPT to force supernumerary cone genesis (Fig S7). Nonetheless, we still did not observe Cherry expression in the retina. Although mouse Pde6c-3B has activity in mice and humans, the human enhancer sequence only had activity in the human retina.

The Pde6c enhancer requires multiple sequence regions for its activity

The activity of the *Pde6c* intron 8 element and the Pde6c-3B sub-element were equivalent. This suggested that the 101 bp *Pde6c-3B* sequence contains all the sequences necessary for enhancer activity. To determine which sequences were essential for activity, we systematically mutated the element (Mills et al., 2017) (Fig 6A). We used site-directed mutagenesis to replace 10 bp bits of sequence with an equal number of adenines (A), maintaining spacing (Fig 6A). This created ten mutant (Mut) constructs that tiled the 101 bp sequence. These plasmids were co-electroporated into mouse E13.5 retinal explants and cultured for 2 DIV. Sections from the explants were immunostained for GFP, RFP (Cherry), and OTX2 (Fig 6B–F', S8). We observed that most of the mutant plasmids (Mut 1–2, 6–10) lacked GFP activity (Fig 6A–F', S8). However, three of the mutant constructs (Mut 3–5) showed GFP expression in the outer-most aspect of the retina (Fig 6A, C–E'). We quantified GFP overlap with OTX2 and found that nearly all of the GFP+ cells in Mut 3–5 co-expressed OTX2 (means = 95, 98, and 98%) (Fig 6C–E', G). This overlap was compared to the parental construct (Pde6c-3B) and to the full intron 8 element. There was no significant difference in OTX2 overlap between these plasmids using Kruskal-Wallis one-way ANOVA with Dunn's multiple comparison tests ($P > 0.05$) (Fig 6G). This argues that each of these mutant constructs behaves equivalently to the parental plasmids. We next immunostained the Mut 3–5 electroporated retinas with RXRG to determine what fraction of the GFP+ cells were cones (Fig 6C', D', E' insets). As with the parental and intron 8 elements, we found that most of the GFP+ cells co-expressed RXRG (means = 78, 93, and 88%) (Fig 6H). The overlap between GFP and RXRG was not statistically different between any of the mutant or parental constructs. Together, this suggests that the sequences in the

Mut 3, 4, and 5 regions are dispensable for enhancer activity (Fig 6I). The Mut 3 construct displayed more variability than the other two mutants. This appeared to be the result of having fewer GFP+ cells than the other two mutants. This could be due to experimental variation or the result of the mutation reducing the number of cells that can activate GFP.

To gain finer resolution in the mutation map, we created several additional 6 bp mutations. These replaced the sequence with 6 A's. Four of these mutations (Mut 11–14) narrowly spanned the junctions between mutants 6–10 (Fig 6A). The other two mutations (Mut 1A, 2A) were designed to narrowly perturb potential binding sites for bHLH transcription factors and for OTX2/CRX (see below) (Fig 6A). All 6 constructs were screened in retinal explants as described above. None of these mutant constructs showed GFP expression in retinal explants (Fig 6, S8). Combined with the first ten mutants, these data suggest that multiple binding sites are necessary for enhancer activity (Fig 6A). These cluster into two regions separated by a gap of unnecessary sequence (Fig 6I). Using JASPAR (Castro-Mondragon et al., 2021), we searched for potential transcription factor binding sites within the required sequence regions. This revealed two E-box sites, which are typically bound by bHLH transcription factors (de Martin et al., 2021; Murre et al., 1994) (Fig 6I). It also predicted an OTX2/CRX site adjacent to the unnecessary sequence region (Fig 6I). Predictions in the large 3' required region were not as simple. Nonetheless, we identified potential FOX, NFAT, and ZBTB family transcription factor binding sites in this region (Fig 6I).

We then examined the *Pde6c-3B* sequence for conservation across genomes (Fig S9). As expected, the unnecessary sequence region showed little conservation across mammals (Fig S9). The necessary sequence regions showed only pockets of high conservation (Fig S9). Compared to the human sequence, there was strong conservation in the 3' predicted bHLH site and in the sequence with potential FOX, NFAT, and/or ZBTB factor binding (Fig S9, S10). The 5' bHLH site had a different core sequence between mice (CAGCTG) and humans (CACTTG) and the OTX2/CRX site was only modestly conserved (Fig S9). Despite these sequence differences in predicted essential binding sites, the mouse sequence drove expression in the human retina. It is unclear why the longer human *PDE6C* sequence was inactive in mice.

Discussion

It is likely that the gene regulatory network that controls cone fate overlaps with the network that governs early cone-specific expression. Since fate specification can occur as a one-time event, we hypothesized that transiently expressed cone-specific enhancers will be regulated by the factors that determine cone fate choice. Our objective was to identify and dissect the function of enhancers that drive transient expression in nascent cone photoreceptors. We determined that a DNA sequence within intron 8 of the mouse *Pde6c* gene was sufficient to drive transient expression in early developing murine cones. This mouse enhancer and its corresponding human sequence each drove equivalent expression patterns within developing cones of human retinal organoid cultures. A dissection of the essential sequences of the *Pde6c* enhancer implicated several regulatory pathways that may control cone fate choice. Further work is needed to uncover how this enhancer functions and how the decision to adopt cone photoreceptor fate is made. In addition, our creation of transgenic iPSCs

provides a new tool to study the differences between mouse and human cone development, which is important for realizing potential human cone-based therapeutics for the treatment of retinal degenerative diseases.

A sequence within intron 8 of Pde6c acts as an early cone-enriched enhancer.

We screened two accessible chromatin regions (Aldiri et al., 2017) within the mouse *Pde6c* gene. The intron 1 ATAC-seq peak was not prominent until later stages, but was retained into maturity. This raises the possibility that the intron 1 sequence acts as a cone-specific enhancer within the mature retina. This possibility is supported by ATAC-seq data from mature photoreceptors (Murphy et al., 2019), which show a prominent intron 1 peak within cones (Fig S2). We examined E13.5 retinal explants electroporated with intron 1 reporter plasmids after 14 days of culture, but did not observe any enhancer activity (data not shown). This suggests that the intron 1 element does not act as an enhancer or that it is only active later in fully mature cones. The ATAC-seq peaks for intron 8 were present early and diminished as the retina aged. This matches the early and transient activity of the intron 8 element in our experiments.

In both mouse and human retinal organoid systems, the intron 8 enhancer expression pattern was restricted to OTX2+ developing photoreceptors. Reporter assays and lineage tracing demonstrated that enhancer activity was strongly biased towards cone photoreceptors. This incomplete cone specificity suggests that the intron 8 enhancer is activated close to when a photoreceptor competent cell decides to commit to cone fate (Fig 7A). The bipolar cell enhancer of *Vsx2* (Kim et al., 2008) appears to act similarly. Lineage tracing this enhancer yields a highly bipolar cell enriched population, but about 10% of the cells adopt rod fate (Goodson et al., 2020a; Goodson et al., 2020b). This is consistent with cells being poised between bipolar and rod photoreceptor fates. Together, these findings suggest a model where competent OTX2+ cells are poised between identities and instructive signals tip the balance to select a fate choice (Fig 7A). Another model posits that cones are a default outcome that is subsequently overridden to generate rods in mammals (Brzezinski and Reh, 2015; Kim et al., 2016). In this model, rods could derive from a pool of OTX2+ cells that initiate cone marker expression. We and others observed cells that co-expressed rod and cone markers (Buenaventura et al., 2019; Chen et al., 2005; Haider et al., 2006; Jean-Charles et al., 2018; Kim et al., 2016; Ng et al., 2011), supporting this model. However, the low number of rods seen in our transgenic human organoids and mouse lineage tracing experiments argues that if there is a cone default state in the retina, it exists upstream of the activation of the *Pde6c* intron 8 enhancer. How photoreceptor competent OTX2+ cells decide to activate the *Pde6c* enhancer and decide between rod and cone fates remains to be fully elucidated.

Transcriptional regulation of the Pde6c enhancer

To uncover which transcription factors regulate the *Pde6c* intron 8 enhancer, we performed enhancer mutagenesis and predicted transcription factor binding sites using JASPAR. Mutation of the 101bp Pde6c-3B minimal enhancer revealed two blocks (20bp and 51bp) that were necessary for expression flanking a dispensable central area (30bp) (Fig 7C, S9). The 20bp upstream region contained an E-box site for bHLH transcription factors and a potential binding site for OTX2/CRX. Based on the four mutants we screened (Mut 1, 1A,

2, and 2A), it is likely that these are the only two requisite transcription factor binding sites in the upstream region. The 51bp downstream essential sequence region also contained an E-box along with overlapping binding predictions for FOX, NFAT, and ZBTB families of transcription factors. The downstream sequence is long enough to contain more than two predicted binding sites. Mutants 9, 10, and 14 all perturb the potential downstream (3') bHLH binding site. It is possible that there is only one transcription factor binding site covered by the overlap of these three mutants. Alternatively, the extreme 3' end of this sequence could contain another binding site. However, this sequence region is only modestly conserved (Fig S9, S10). The 33bp region covered by mutants (Mut 6–8, 11–13) likely includes multiple transcription factor binding sites. This is because no single binding site (less than 19 bp long) could be perturbed by all six mutant constructs. Based on the JASPAR predictions within this 33bp region, it is likely that there are at least two transcription factor binding sites for a combination of FOX, NFAT, and/or ZBTB factors. Taken together, the mutagenesis data suggest that at least five potential transcription factor binding sites are needed for Pde6c-3B enhancer activity in developing cones (Fig 7C).

Which transcription factors bind these five predicted sites during retinal development? Answering this question is challenging due to the high number of factors that could potentially bind these sites and the possibility that the JASPAR predictions are incomplete or fail to reflect what is actually bound in cells. Developmental and gene expression profiling studies support a regulatory role for all five predicted transcription factor families. Most conspicuous is a role for the homeodomain transcription factors OTX2 and CRX (Fig 7B), which have a lysine at residue 50 (K50) of their homeodomain (Burglin and Affolter, 2016; Lee et al., 2010). Both factors are expressed early in photoreceptor development (Chen et al., 1997; Furukawa et al., 1997; Muranishi et al., 2011; Nishida et al., 2003). *Otx2* is required for photoreceptor formation while *Crx* acts downstream and is needed for photoreceptor maturation and homeostasis (Furukawa et al., 1999; Ghinia Tegla et al., 2020; Nishida et al., 2003; Sato et al., 2007; Yamamoto et al., 2020) (Fig 7B). Based on their early expression and critical involvement in photoreceptor development and function, OTX2 and/or CRX are likely necessary for *Pde6c* enhancer activity. Both factors are made by mature rods and cones, which indicates that these factors are not sufficient for the transient cone-enriched enhancer pattern we observed.

The bHLH transcription factor family contains many members, several of which are made at the right time and place to regulate *Pde6c* enhancer activity (Kaufman et al., 2019; Skinner et al., 2010). We observed that bHLH factors can act in a redundant or compensatory fashion to regulate retinal enhancer activity (Kaufman et al., 2021). These features make it difficult to predict which bHLH factor binds a given E-box (CANNTG) site. However, there is a binding preference based on the E-box half-site sequence (CAN) (de Martin et al., 2021). Some bHLH factors, such as ASCL1 and PTF1A, have a binding preference for E-boxes that contain CAG half-sites while others, such as NEUROD1 and ATOH7, preferentially bind to CAC half-sites (de Martin et al., 2021). The upstream (5') E-box in the Pde6c-3B enhancer contains symmetrical CAG half-sites while the downstream E-box has symmetrical CAC half-sites. This raises the possibility that these sites are bound by distinct bHLH transcription factors. A strong candidate regulator of the downstream E-box is NEUROD1 (Fig 7B). *Neurod1* mutant photoreceptors do not function normally and have

reduced expression of some cone markers, such as THRB and M-OPSIN (Liu et al., 2008; Pennesi et al., 2003). NEUROD1 directly binds to an intronic enhancer of the *Thrb* gene that drives a cone-enriched expression pattern in the retina (Emerson et al., 2013; Jones et al., 2007; Liu et al., 2008). These data are consistent with NEUROD1 regulating a cone-specific program during retinal development (Fig 7B). Although NEUROD1 is a strong candidate for regulating the *Pde6c* enhancer, it is broadly expressed by developing photoreceptors and amacrine cells (Morrow et al., 1999). Like OTX2 and CRX, NEUROD1 does not appear to be sufficient to convey a transient cone-enriched enhancer activity pattern. It is likely that other bHLH factors regulate *Pde6c* enhancer activation, especially at the upstream E-box that contains the CAG half-site. Which factors, whether they restrict spatial and temporal activity to cones, and whether they function in a redundant or compensatory fashion is unknown. To explore this further, we examined the small number of transcription factor chromatin immunoprecipitation sequencing (ChIP-seq) datasets generated from the developing mouse retina (Fig S11). However, we did not observe binding of ASCL1 (Jorstad et al., 2020), ATOH7 (Brodie-Kommit et al., 2021), or other transcription factors at the *Pde6c* intron 8 enhancer (Fig S11).

Discovering which transcription factors regulate the 33bp region predicted to bind FOX, NFAT, or ZBTB family members is also challenging. Since no ChIP-seq datasets are available for these transcription factors in the developing retina, we asked whether any factors from these families were expressed at the right time and place to regulate *Pde6c* enhancer activity. To do this, we browsed single cell RNA-sequencing data from developing mouse retinas (Clark et al., 2019) available online (eyeintegration.nei.nih.gov). We focused on the “photoreceptor precursor” and “cone” cell fate categories in this dataset because they are likely to coincide with *Pde6c* enhancer activity. Members from all three families are expressed in the “photoreceptor precursor” or “cone” categories. Several examples were seen for the forkhead domain (FOX) (Hannenhalli and Kaestner, 2009) and C2H2 zinc finger domain (ZBTB) (Cheng et al., 2021; Maeda, 2016) transcription factor families, which have many members. Although lacking JASPAR predictions, it is also possible that other transcription factor subfamilies implicated in cone fate choice, such as ONECUT, POU2F, LHX, and IKZF (Fig 7B), bind to this 33bp region (Buenaventura et al., 2019; Elliott et al., 2008; Emerson et al., 2013; Javed et al., 2021; Javed et al., 2020; Sapkota et al., 2014). Whether any of these factors bind the *Pde6c* enhancer or explain its narrow spatial and temporal pattern is unknown.

Gene regulatory networks involved in cone development

The gene regulatory network that controls cone genesis is only partially understood (Fig 7B). Initial efforts to find early cone-enriched enhancers focused on the *Thrb* gene, the β2 isoform of which is made by developing cones (Fig 7B) (Ng et al., 2001; Sjoberg et al., 1992). An intronic sequence (ThrbICR) downstream of the β2-specific exon drives a cone-enriched pattern of expression embryonically and into adulthood in mice (Emerson et al., 2013; Jones et al., 2007). Two other enhancers upstream of the β2-specific exon were defined in chick, termed ThrbCRM1 and ThrbCRM2 (Emerson et al., 2013). Lineage tracing studies performed in chick showed that the ThrbICR and ThrbCRM1 enhancers predominantly marked developing cones and horizontal cells, whereas the ThrbCRM2

enhancer was highly cone-specific (Schick et al., 2019). Similar to ThrbCRM1, an enhancer close to the chick *Rxrg* gene (Rxrg208) drove expression in developing cones (Fig 7B) and horizontal cells (Ameixa and Brickell, 2000; Blixt and Hallbook, 2016). OTX2 was shown to be required for ThrbCRM1 and Rxrg208 enhancer activity (Emerson et al., 2013; Lonfat et al., 2021; Souferi and Emerson, 2019) and the ThrbICR enhancer was regulated by NEUROD1 (Liu et al., 2008). All three of these enhancers were regulated by ONECUT subfamily transcription factors (Fig 7B) (Emerson et al., 2013; Lonfat et al., 2021; Souferi and Emerson, 2019). Multiple enhancers near the *Onecut1* gene in chick had cone-enriched expression patterns in the retina (Patoori et al., 2020). Several of these enhancers appear to be regulated by distinct sets of bHLH transcription factors (Patoori et al., 2020). More recently, genomic approaches have been used to infer gene regulatory networks involved in photoreceptor development and homeostasis (Cherry et al., 2020; Finkbeiner et al., 2022; Hughes et al., 2017; Lonfat et al., 2021; Lyu et al., 2021; Murphy et al., 2019; Perez-Cervantes et al., 2020). An examination of open chromatin regions in developing chick cones strongly implicated OTX2, ONECUT, and bHLH transcription factors in their genesis (Lonfat et al., 2021). Single-cell level analyses of accessible chromatin regions during mouse and human retinal development identified several binding site motifs enriched in developing cones (Finkbeiner et al., 2022; Lyu et al., 2021). These included E-boxes, GATA, nuclear receptor, IKZF, ZBTB, MEIS, ONECUT, and K50 and Q50 homeodomain transcription factor binding sites (Finkbeiner et al., 2022; Lyu et al., 2021).

The results of these experiments strongly implicate OTX2, ONECUT, and bHLH transcription factors in cone enhancer regulation and cone fate specification (Fig 7B). A role for other transcription factors recently implicated in cone formation, such as IKZF and POU2F (Elliott et al., 2008; Javed et al., 2021; Javed et al., 2020) (Fig 7B), are also supported by these findings. Our regulatory predictions for the *Pde6c* intron 8 enhancer only partially match these results. The *Pde6c* enhancer has strong binding predictions for OTX2/CRX and bHLH factors, but lacks them for IKZF, POU2F, or ONECUT factors. The studies noted above provide evidence for ZBTB factor involvement, but little for FOX or NFAT transcription factors. This may indicate that ZBTB, FOX, and NFAT pathways are heretofore unappreciated regulators of cone development. Another possibility is that early cone-enriched enhancers utilize a combination of shared and distinct regulatory mechanisms to govern their expression. Whether shared or distinct, cone enhancer regulation is likely to be further complicated by issues of transcription factor redundancy or compensation.

Differences between mouse and human enhancer sequences

Gene expression profiling suggests that cones are the retinal cell type with the most transcriptional differences between mice and humans (Lu et al., 2020). This is paralleled by recent findings showing that cone-specific accessible chromatin peaks have lower conservation than other cell types between species (Lyu et al., 2021). This suggests that the gene regulatory networks that control cone development are similar, but not identical, between mice and humans. Differences in how the gene regulatory network functions would likely be encoded at the enhancer level. The similarities and differences between the human and mouse *Pde6c* enhancer sequences and their activity may help answer two

broad questions: (1) how do nucleotide changes lead to new regulatory logic, and (2) how tolerant are gene regulatory networks to changes in enhancer DNA sequence?

The human and mouse *Pde6c* enhancers had equivalent expression patterns in developing cones. The mouse enhancer labeled cones in mouse and human retinas, while the human enhancer only had activity in human tissue. Comparing the sequence of the mouse *Pde6c-3B* region with human, we found only moderate conservation (Fig S9, S10). In general, the required sequences in the downstream region showed higher conservation than the upstream regions (Fig S9). Particularly striking was the change in the core of the upstream E-box to have asymmetric half-sites (CAC & CAA) and the breakdown of the potential OTX2/CRX K50 homeodomain binding site in human (Fig S9, S10). With limited sequence conservation, how do the human and mouse enhancers drive such similar expression patterns? One possibility is that the same types of binding sites are used to regulate expression in each species, but they are arranged in a different order, number, or spacing (Fig 7D). This would lower sequence conservation while grossly maintaining the overall regulatory logic. This may be occurring with the potential OTX2/CRX and bHLH binding sites. OTX2 chromatin immunoprecipitation experiments in the adult mouse retina defined a core binding site of TAATCC (GGATTA on the other strand), with some flexibility in positions 4 and 6 for other nucleotides (Samuel et al., 2014). Downstream of the conserved region with *Pde6c-3B* is a potential OTX2 binding site with the sequence of TAAGCT (AGCTTA on the other strand) (Fig S10). This has the lower frequency G and T nucleotides at positions 4 and 6 (Samuel et al., 2014), respectively, and may function as an OTX2 binding site in the human *PDE6C* sequence. The upstream E-box in mouse containing the symmetric CAG half-sites is not seen in the human *PDE6C* sequence region. However, the human enhancer has three additional E-boxes-two downstream of the *Pde6c-3B* conserved region and one that is only a few base pairs downstream of the potential OTX2/CRX binding site (Fig S10). The latter E-box contains an asymmetric CAG half-site (Fig S10), which could allow for the same types of bHLH transcription factors to bind both mouse and human enhancer sequences. Although binding sites may ultimately be conserved between species, a shared regulatory logic model does not explain why the human enhancer lacks activity in mice. This raises the possibility that there are differences in regulatory logic between species (Fig 7D). Distinct regulatory mechanisms would further explain why enhancer conservation is modest between species. In this scenario, there would be some differences in which transcription factors are used to regulate the *Pde6c* enhancer in each species (Fig 7D). This model would explain why the human enhancer sequence does not function in mice. However, it does not explain why the mouse enhancer has activity in human retinal organoids. Activity may occur because human retinas express transcription factors that compensate for the sequence differences in the mouse enhancer. Finally, it is possible that cone-enriched enhancers contain a high degree of binding site flexibility and shared regulatory logic, yet have a small number of species-specific regulatory aspects (Fig 7D).

Determining which aspects of *Pde6c* enhancer regulatory logic are flexible, shared, and distinct will require a series of enhancer mutagenesis experiments screened in the human organoid system. Dissection of how enhancers function between species will help us understand how much flexibility is present in gene regulatory networks and how they evolve to control shared developmental events. Understanding how gene regulatory networks

function in human retinas will also be important for successfully implementing strategies that utilize human iPSC-derived cones for regenerative medicine purposes.

Materials and Methods

Animals

All animal work was conducted with approval from the University of Colorado Anschutz Medical Campus IACUC. Retinal explants collected from *CD-1* mouse embryos (Charles River Laboratories, Wilmington, MA, USA) were used for the majority of experiments. For lineage tracing experiments, explants were derived from *Gt(ROSA)26Sor*$^{tm14(CAD\text{-}tdTomato)Hze}$ (strain #7914) reporter mouse embryos (Jackson Laboratories, Bar Harbor, ME, USA) (Madisen et al., 2010). We refer to these animals as *ROSA-RFP*. The morning a vaginal plug was observed was considered embryonic (E) day 0.5. To create *Pde6c-GFP-Cre* transgenic mice, we purified linearized plasmid lacking the backbone vector sequences (origin of replication and the drug resistance gene). With the assistance of the University of Colorado Denver Bioengineering Core, this vector was used for standard pronuclear injection on the *C57BL/6* background. Three rounds of pronuclear injection were completed, but only three female founders were generated. One founder did not breed and the other two failed to transmit the transgene. Ultimately, we were unable to establish a *Pde6c-GFP-Cre* line.

Enhancer identification, binding site predictions, and plasmid tool generation

We utilized ATAC-sequencing data from whole developing retina (Aldiri et al., 2017) displayed on the UCSC Genome Browser to identify regions of accessible chromatin surrounding the mouse *Pde6c* gene. ATAC-sequencing data from mature rod and cone photoreceptors (Murphy et al., 2019) was displayed on the UCSC Genome browser and used to gauge the cell-type specificity of the peaks. In the space (~63kb) between the genes flanking *Pde6c*, four prominent ATAC peaks were observed (Fig S1). We screened the peaks within introns 1 and 8 for activity in the retina. The two peaks upstream of *Pde6c* were not evaluated due to their close proximity to the transcription start site (Fig S1). For transcription factor binding site predictions, we utilized JASPAR 2022 (Castro-Mondragon et al., 2021) loaded as a track in the UCSC genome browser (*mm10* and *hg38* assemblies). The track score minimum was set to 350 to have relatively high stringency. Binding site predictions were simplified to transcription factor families.

To evaluate ATAC-seq peaks for enhancer activity, we independently inserted intron 1 and intron 8 peak sequences into plasmids containing a minimal TATA promoter driving nuclear-localized (n) GFP (pMin-nGFP) as previously described (Kaufman et al., 2021; Mills et al., 2017; Wilken et al., 2015). Briefly, In-Fusion HD cloning (Takara, San Jose, CA, USA) was used to insert potential enhancer sequences upstream of the TATA promoter in pMin-nGFP (Supplemental Table 1). Control plasmids to label all electroporated cells included the ubiquitous *EF1a* promoter driving either nuclear-localized monomeric (m) Cherry (a red fluorescent protein- RFP) or cytoplasmic GFP (Kaufman et al., 2021; Mills et al., 2017; Wilken et al., 2015). The empty pMin-nGFP plasmid without any enhancers (TATA-only) served as a negative control. To make short mutations in plasmids, we used

the In-Fusion site-directed mutagenesis protocol (Takara) (Kaufman et al., 2021; Mills et al., 2017). The endogenous enhancer sequence was altered in 6 or 10 bp stretches to convert it into a string of adenines (A). The overall length of the sequence was maintained in these mutant constructs. See Supplemental Table 1 for the sequences of all enhancer constructs in pMin-nGFP.

To build lineage tracing plasmids, we utilized a previously generated construct that drives co-expression of GFP and Cre recombinase (Goodson et al., 2020b; Kaufman et al., 2021). This was adapted from the pMin-nGFP plasmid to include a self-cleavage peptide and Cre recombinase cassette downstream of nGFP (pMin-nGFP-2A-Cre) (Goodson et al., 2020b). We used In-Fusion cloning to insert the human *EF1a* (*EEF1A1*) promoter region or the *Pde6c* intron 8 sequence (Supplemental Table 1) upstream of the minimal TATA promoter to generate the final lineage tracing plasmids.

Two targeting plasmids were made to conduct cassette exchange in AAVS1-copGFP iPSCs (Fig S6) (Pei et al., 2015). These were based on the ZYP068 plasmid created by Pei and colleagues (Pei et al., 2015). ZYP068 contains Lox2272 and Lox511 sites flanking a cloning site, a TagGFP cassette, and a PGK-Neomycin resistance cassette. We first modified ZYP068 to remove the TagGFP cassette. This was done by cutting the plasmid with *Nhe*I and *Afl*II, using Klenow fragment to make blunt ends, and ligating the blunt ends with Quick Ligase (NEB, Ipswich, MA, USA). This plasmid, ZYP068-ΔGFP, retained its *Nhe*I and *Afl*II sites. In parallel, we modified our pMin-nGFP plasmid to replace nGFP with nCherry. Due to the lack of easily available restriction sites flanking the fluorescent reporter, the replacement of nGFP with nCherry was performed by inverse PCR of the pMin-GFP plasmid followed by In-Fusion cloning of a PCR amplified mCherry fragment containing two strong nuclear localization signals at its C-terminus. Taking advantage of the sequence homology between the proximal and distal ends of both reporter colors, we first inverse PCR amplified within the GFP sequence using 5`-TCCTCGCCCTTGCTCACCAT and 5`-GGCATGGACGAGCTGTACAAG primers to generate an empty pMin backbone. Next, an internal sequence of mCherry was PCR amplified from pLVX-mCherry (632561, Takara Bio USA) using 5`-ATGGTGAGCAAGGGCGAGGA and 5`-CTTGTACAGCTCGTCCATGCC primers. The purified products of these reactions were combined following the standard In-Fusion protocol. The resulting plasmid, pMin-nCherry, has the same cloning sites upstream of the minimal TATA promoter as the parental pMin-nGFP construct. We then PCR amplified a portion of pMin-nCherry to include the cloning sites, the TATA promoter, nCherry, and its polyadenylation (pA) signal sequence. In-Fusion cloning was used to insert this amplicon into the *Nhe*I and *Afl*II sites of ZYP068-ΔGFP. This resulted in ZYP068-min-nCherry. Finally, we used In-Fusion cloning to insert mouse *Pde6c-3B* or the human *PDE6C* sequence (Supplemental Table 1) upstream of the TATA box between the *Nhe*I and *Sac*II sites of ZYP068-min-nCherry. This resulted in the two targeting plasmids that were used to make transgenic iPSC lines (below) (Fig S6).

We also utilized the pMin-nCherry construct to screen the human *PDE6C* element (Supplemental Table 1) in mice. For this, In-Fusion cloning was used to insert the human sequence into the *Sac*I and *Kpn*I sites in the vector. As an electroporation control, we used

previously generated plasmids that ubiquitously express both Cas9 and cytoplasmic GFP from the *EF1a* promoter (Kaufman et al., 2021).

Sanger sequencing was used to validate all plasmids generated in this project. In-Fusion primers for insertions and mutagenesis were generated with the online design tool from Takara. Plasmid maps were managed with Benchling (Benchling.com).

Electroporations and explant culturing

To screen enhancer activity and conduct lineage tracing, embryonic mouse retinas from *CD-1* or *ROSA-RFP* mice were dissected, electroporated, and cultured as explants as described previously (Kaufman et al., 2021; Mills et al., 2017). Eyes from E13.5 or E14.5 embryos were dissected in cold Hank's Balanced Salt Solution (HBSS with Ca^{2+} and Mg^{2+}) (Corning, Corning, NY USA) supplemented with 0.05 M HEPES and 6 mg/mL glucose. The eyes were further dissected to leave the retina and lens intact. Next, 1–2 μL of plasmid DNA mixture (1:1 mix of control and experimental plasmids at 3 μg/μL final concentration) was added to the photoreceptor side of the retinas. For lineage tracing, one plasmid was electroporated at a 2 μg/μL final concentration. Two to four retinas were electroporated simultaneously with five square wave pulses of 50 V for 50 ms with 250 ms intervals with a Bio-Rad Gene Pulser Xcell (Bio-Rad, Hercules, CA, USA). The electroporated explants were placed in a 12-well plate with 2 mL growth media [Neurobasal Medium containing 1X N2 supplement, 1X L-glutamine, 1X penicillin/streptomycin, and 1% fetal bovine serum (FBS)] (Gibco/Thermo Fisher Scientific, Waltham, MA, USA). Explants were cultured under 5% CO_2 in a 37°C incubator using a nutator at 12 RPM to gently oxygenate them for up to 2 DIV (days *in vitro*). For experiments using γ-secretase inhibitors, we added 10 μM DAPT (N-[N-(3,5-Difluorophenacetyl-L-alanyl)]-S-phenylglycine t-Butyl Ester) (565770, Millipore Sigma, Burlington, MA, USA) or the equivalent volume of DMSO vehicle (1 part per thousand) to the cultures for 2 DIV as done previously (Kaufman et al., 2019). For cultures grown 7 or 14 DIV, explants were electroporated as above, the lens removed, and the retina flattened ganglion-side down onto Omnipore membrane filters (0.45μm) (Millipore Sigma). These were then transferred onto 30 mm diameter 0.4 μm Millicell CM cell culture inserts (Millipore Sigma) in a 6-well plate. The flattened explants were cultured at the air-media interface in growth media containing 10% FBS. These explants were also grown under 5% CO_2 in a 37°C incubator, but without nutation. Half of the media was changed every other day.

Transgenic iPSC line construction

Genetically modified undifferentiated human iPSCs containing a ubiquitously expressed GFP cassette inserted at the *AAVS1* safe harbor locus (AAVS1-copGFP) (Pei et al., 2015) were grown to sub-confluency on Matrigel (354234, Corning) coated 6-well plates with mTeSR Plus medium (100–0274, STEMCELL Technologies, Vancouver, BC, Canada). AAVS1-copGFP human iPSCs were dissociated by incubating cells in 0.5 mM EDTA (46–034-Cl, Corning) in 1X DPBS (21–031-CV, Corning) for 4 to 5 minutes. This dissociation media was removed. Next, the cells were gently scraped in DPBS, transferred into a 15 mL tube, and spun at 1200g for 3 minutes. The cells were resuspended in 1X DPBS and viable cell count was determined using a trypan blue dye (0.4%) exclusion method (Countess II

FL, Thermo Fisher Scientific). About 400 to 700 thousand cells were resuspended in 200 µL of freshly prepared sterile electroporation buffer [140mM $Na_2HPO_4 \cdot 7H_2O$ (S2429–250G, Sigma), 15mM $MgCl_2 \cdot 6H_2O$ (M2393–500G, Sigma), 5mM KCl (P5405–500G, Sigma), 25mM D-Mannitol (M-4125–100G, Sigma), and 15mM HEPES (25–060-Cl, Corning)]. The Cre (Addgene plasmid #24593, a gift from Dr. Patrick Aebischer) and targeting plasmids (mPde6c-3B-nCherry, hPDE6C-nCherry, see above) were prepared using an endotoxin-free Plasmid Maxiprep Kit (12362, Qiagen, Germantown, MD, USA), quantified using a Nanodrop One (Thermo Fisher Scientific) and stored at 2.5 – 6 µg/mL in sterile TE, pH 8.0. The cells resuspended in electroporation buffer were mixed with plasmid vectors in two combinations: (1) Cre (~13 µg) and mPde6c-3B (~15 µg), or (2) Cre (~13 µg) and hPDE6C (~15 µg). Transfection was performed by transferring the mixture into 2 mm-gap cuvettes (Lonza, Basel, Switzerland) and the cells electroporated using the B-016 program on an Amaxa Nucleofector II System (Lonza). Electroporated cells from the cuvette were then cultured on Matrigel-coated 6-well plates in mTeSR Plus media. The media was changed 24 hours after plating and then every other day. After 4–5 days of electroporation, cells were treated with 200 µg/mL of the neomycin analog G418 (MIR5920, Thermo Fisher Scientific) for 5 days (with daily drug/media changes) to select cells that underwent cassette exchange (Fig S6). Cell clusters identified by brightfield microscopy that lacked GFP expression were picked manually and transferred to Matrigel-coated 12-well plates. The clones were grown to confluence and screened further by PCR. Genomic DNA was extracted (DNeasy Kit, 69504, Qiagen) from the expanded transgenic clones. PCR was conducted to confirm the absence of copGFP and the presence of nCherry. The primers used were GFP-F 5’-CGCATGACCAACAAGATGAAG, GFP-R 5’-GGCAGAATTGGACGACTGA, Cherry-F 5’-TTCATGTACGGCTCCAAGGC, and Cherry-R 5’-CTGCTTGATCTCGCCCTTCA. Products were amplified using 2 µL of DNA and Dream Taq Green PCR mix (K108, Thermo Fisher Scientific) under the following conditions: initial denaturation of 94°C (4 minutes), then 36 cycles of 94°C (30”), 60°C (60”), 72°C (30”), and 1 cycle of 72°C (7 minutes). PCR amplicons were detected by gel electrophoresis in 1% agarose gels containing a few drops of EZ-Vision® In-Gel Solution (N391, VWR Life Science, Radnor, PA, USA) and photographed using a Bio-Rad GelDoc XR+ Imaging System (Bio-Rad). Multiple iPSC clones were identified for both AAVS1-mPde6c-3B-nCherry and AAVS1-hPDE6C-nCherry lines. One clone for each line was used for organoid experiments.

Retinal Organoid Differentiation and Culturing

Retinal organoids were differentiated using AAVS1-mPde6c-3B-nCherry and AAVS1-hPDE6C-nCherry lines via the embryoid body (EB) approach as described previously (Chirco et al., 2021). Briefly, iPSC colonies used to make retinal organoids were transferred to a 6-well suspension plate as EBs and transitioned gradually into Neural Induction Medium (NIM) containing DMEM/F12 (SH30023.02, HyClone, Logan, UT, USA), 1X MEM nonessential amino acids (25025CI, Corning), 2 mM GlutaMAX Supplement (35050061, Gibco Thermo Fisher Scientific), 2 µg/mL Heparin sulfate (H3393, Millipore Sigma), 1X Penicillin/Streptomycin (30001CI, Corning), and 1X N-2 Supplement (17502001, Gibco Thermo Fisher Scientific). On day 6, EBs were fed with NIM containing 1.5 nM BMP4 (120–05ET, PeproTech, Cranbury, NJ, USA). On day 7, the 3D EBs were transferred onto a Matrigel-coated plate with fresh NIM medium + 1.5 nM BMP4 to

allow EBs to adhere to the plate. The concentration of BMP4 was gradually reduced to 0.375 nM from day 7 to day 14 to promote the differentiation of photoreceptors within the EB. From day 16 through day 29, the EBs were fed Retinal Differentiation Medium (RDM), which contains equal parts DMEM/F12 (SH30023.02, HyClone) and DMEM High Glucose (SH30022.02, HyClone),1X MEM nonessential amino acids, 1X GlutaMAX Supplement, 1X Penicillin/Streptomycin, and 2X B-27 Supplement (17504001, Gibco Thermo Fisher Scientific). Regions of the plate that began to display clear retina-like morphology during this period were manually lifted using a sterile P100 pipette tip. The lifted neural retinas were transferred to a suspension plate and allowed to acquire a 3D organoid structure. From day 30 to day 120, the developing retinal organoids were fed 3D-RDM medium, which is RDM media with 5% Fetal Bovine Serum (S11150, R&D Systems, Minneapolis, MN, USA), 200 μM Taurine (T0625, Millipore Sigma), Chemically Defined Lipid Concentrate (1:1000, 11905031, Gibco Thermo Fisher Scientific), and 1 μM all-trans retinoic acid (R2625, Millipore Sigma). Organoids were collected at days 45, 59, and 120 of differentiation for analysis.

Immunohistochemistry

Retinal tissues were fixed in 2% paraformaldehyde (Electron Microscopy Sciences, Hatfield, PA, USA) in PBS for 20–40 minutes, cryopreserved through 30% sucrose in PBS, and frozen in OCT (Sakura, Torrance, CA, USA) (Brzezinski et al., 2010). Organoids were fixed with 4% paraformaldehyde (Electron Microscopy Sciences) in PBS at 4°C for 20 minutes prior to cryopreservation and embedding in OCT. Tissue was cryosectioned at 10 μm using a Microm HM 550 cryostat (Thermo Fisher). Immunohistochemistry was done as described previously (Brzezinski et al., 2010; Goodson et al., 2020a; Kaufman et al., 2021). Slides were incubated at room temperature for 1–3 hours in milk block solution (the supernatant of 5% milk and 0.5% Triton X-100 in PBS). Primary antibodies were diluted in milk block and then added to the slides overnight (12–18 h) at room temperature or at 4°C for organoid tissues. The slides were washed in PBS and incubated for 1 hour at room temperature with fluorescently conjugated secondary antibodies (Jackson ImmunoResearch, West Grove, PA, USA) diluted 1:500 in milk block solution. The slides were washed in PBS and mounted. Primary antibodies used in this study were: mouse anti-Cre (1:250, MAB3120 Millipore), chicken anti-GFP (1:1000, ab13970, Abcam, Cambridge, UK), mouse anti-NR2E3 (1:250, PP-H7223–00, Perseus Proteomics, Tokyo, Japan), goat anti-NRL (1:200, AF2945, R&D Systems), goat anti-OTX2 (1:250; BAF1979, R&D Systems), rabbit anti-RFP (1:500, ab34771, Abcam), rat anti-RFP (1:500, 5F8–100, Chromotek, Planegg-Marinsried, Germany), mouse anti-RXRG (1:200; sc-365252, Santa Cruz Biotechnology, Dallas, TX, USA), and rabbit anti-RXRG (1:200, sc-555, Santa Cruz Biotechnology). Of note, both anti-RFP antibodies robustly detected monomeric Cherry, but only the rabbit anti-RFP antibody detected tdTomato from *ROSA-RFP* mice.

Imaging, quantification, and statistics

Immunostained sections from mice were imaged with a Nikon C2 laser scanning confocal microscope (Nikon, Melville, NY, USA). Images were captured as a 1024×1024 pixel area with 3–5 z-stacks (1–1.5 μm per slice). The images were flattened by maximum intensity projection in ImageJ (Schneider et al., 2012) and the levels minimally processed

using Adobe Photoshop (Adobe Systems, San Jose, CA, USA). For human organoid immunostaining, images were acquired using ZEN software on an inverted confocal microscope (Carl Zeiss LSM700) and processed by ImageJ (NIH, USA). For all images, cell numbers were quantified manually by channel (antibody) and overlaps calculated and recorded in Microsoft Excel (Microsoft, Redmond, WA, USA). For comparisons between conditions, non-parametric statistical tests were performed in Prism 9.3.0 (GraphPad, San Diego, CA, USA). In cases where multiple groups were compared, Kruskal-Wallis one-way ANOVA was performed followed by Dunn's Multiple Comparison tests between all pairwise groups. In cases where only two conditions were compared, 2-tailed Mann-Whitney tests were used. For all cases, $P < 0.05$ was considered significant. All plots were generated using Prism 9.3.0, such that dots represent individual quantified images. The biological sample size N (number of explants or organoids) and technical sample size n (number of images) are listed in each figure caption.

Supplementary Material

Refer to Web version on PubMed Central for supplementary material.

Acknowledgements

The authors thank the University of Colorado Bioengineering Core for assistance with transgenic mice and Xianmin Zeng for the ZYP068 plasmid and the AAVS1-copGFP iPSC line. The authors thank Noah Goodson, Canaan Kerr, Ian Purvis, and Omar Ochoa for technical advice and for critically reading the manuscript. Work was supported, in part, by grants from the National Institutes of Health (R01-EY024272 to J.A.B and U24-EY029891 and R01-EY032197 to D.A.L.). V.B. was supported by a Challenge Grant from the Boettcher Foundation. Work was partially supported by an Unrestricted Grant to the University of Colorado Department of Ophthalmology from Research to Prevent Blindness. Work was partially supported by a P30 Vision Core grant to the UCSF Dept of Ophthalmology (P30-EY002162), Research to Prevent Blindness (unrestricted grant to UCSF Dept of Ophthalmology), and a gift from the Claire Giannini Foundation to D.A.L.

References

Akimoto M, Cheng H, Zhu D, Brzezinski JA, Khanna R, Filippova E, Oh EC, Jing Y, Linares JL, Brooks M, et al. (2006). Targeting of GFP to newborn rods by Nrl promoter and temporal expression profiling of flow-sorted photoreceptors. Proc Natl Acad Sci U S A 103, 3890–3895. [PubMed: 16505381]

Aldiri I, Xu B, Wang L, Chen X, Hiler D, Griffiths L, Valentine M, Shirinifard A, Thiagarajan S, Sablauer A, et al. (2017). The Dynamic Epigenetic Landscape of the Retina During Development, Reprogramming, and Tumorigenesis. Neuron 94, 550–568 e510. [PubMed: 28472656]

Ameixa C and Brickell PM (2000). Characterization of a chicken retinoid X receptor-gamma gene promoter and identification of sequences that direct expression in retinal cells. Biochem J 347, 485–490. [PubMed: 10749678]

Applebury ML, Antoch MP, Baxter LC, Chun LL, Falk JD, Farhangfar F, Kage K, Krzystolik MG, Lyass LA and Robbins JT (2000). The murine cone photoreceptor: a single cone type expresses both S and M opsins with retinal spatial patterning. Neuron 27, 513–523. [PubMed: 11055434]

Baas D, Bumsted KM, Martinez JA, Vaccarino FM, Wikler KC and Barnstable CJ (2000). The subcellular localization of Otx2 is cell-type specific and developmentally regulated in the mouse retina. Brain research. Molecular brain research 78, 26–37. [PubMed: 10891582]

Baden T, Schubert T, Chang L, Wei T, Zaichuk M, Wissinger B and Euler T (2013). A tale of two retinal domains: near-optimal sampling of achromatic contrasts in natural scenes through asymmetric photoreceptor distribution. Neuron 80, 1206–1217. [PubMed: 24314730]

Bassett EA and Wallace VA (2012). Cell fate determination in the vertebrate retina. Trends in neurosciences 35, 565–573. [PubMed: 22704732]

Blixt MK and Hallbook F (2016). A regulatory sequence from the retinoid X receptor gamma gene directs expression to horizontal cells and photoreceptors in the embryonic chicken retina. Mol Vis 22, 1405–1420. [PubMed: 28003731]

Boije H, MacDonald RB and Harris WA (2014). Reconciling competence and transcriptional hierarchies with stochasticity in retinal lineages. Current opinion in neurobiology 27, 68–74. [PubMed: 24637222]

Brightman DS, Razafsky D, Potter C, Hodzic D and Chen S (2016). Nrl-Cre transgenic mouse mediates loxP recombination in developing rod photoreceptors. Genesis 54, 129–135. [PubMed: 26789558]

Brodie-Kommit J, Clark BS, Shi Q, Shiau F, Kim DW, Langel J, Sheely C, Ruzycki PA, Fries M, Javed A, et al. (2021). Atoh7-independent specification of retinal ganglion cell identity. Sci Adv 7.

Brzezinski JA, Lamba DA and Reh TA (2010). Blimp1 controls photoreceptor versus bipolar cell fate choice during retinal development. Development 137, 619–629. [PubMed: 20110327]

Brzezinski JA and Reh TA (2015). Photoreceptor cell fate specification in vertebrates. Development 142, 3263–3273. [PubMed: 26443631]

Brzezinski JA, Uoon Park K and Reh TA (2013). Blimp1 (Prdm1) prevents re-specification of photoreceptors into retinal bipolar cells by restricting competence. Dev Biol 384, 194–204. [PubMed: 24125957]

Buenaventura DF, Corseri A and Emerson MM (2019). Identification of Genes With Enriched Expression in Early Developing Mouse Cone Photoreceptors. Invest Ophthalmol Vis Sci 60, 2787–2799. [PubMed: 31260032]

Bumsted O'Brien KM, Cheng H, Jiang Y, Schulte D, Swaroop A and Hendrickson AE (2004). Expression of photoreceptor-specific nuclear receptor NR2E3 in rod photoreceptors of fetal human retina. Invest Ophthalmol Vis Sci 45, 2807–2812. [PubMed: 15277507]

Burglin TR and Affolter M (2016). Homeodomain proteins: an update. Chromosoma 125, 497–521. [PubMed: 26464018]

Carter-Dawson LD and LaVail MM (1979). Rods and cones in the mouse retina. II. Autoradiographic analysis of cell generation using tritiated thymidine. J Comp Neurol 188, 263–272. [PubMed: 500859]

Castro-Mondragon JA, Riudavets-Puig R, Rauluseviciute I, Berhanu Lemma R, Turchi L, Blanc-Mathieu R, Lucas J, Boddie P, Khan A, Manosalva Perez N, et al. (2021). JASPAR 2022: the 9th release of the open-access database of transcription factor binding profiles. Nucleic Acids Res.

Cepko C (2014). Intrinsically different retinal progenitor cells produce specific types of progeny. Nature reviews. Neuroscience 15, 615–627. [PubMed: 25096185]

Chen J, Rattner A and Nathans J (2005). The rod photoreceptor-specific nuclear receptor Nr2e3 represses transcription of multiple cone-specific genes. J Neurosci 25, 118–129. [PubMed: 15634773]

Chen S, Wang QL, Nie Z, Sun H, Lennon G, Copeland NG, Gilbert DJ, Jenkins NA and Zack DJ (1997). Crx, a novel Otx-like paired-homeodomain protein, binds to and transactivates photoreceptor cell-specific genes. Neuron 19, 1017–1030. [PubMed: 9390516]

Cheng ZY, He TT, Gao XM, Zhao Y and Wang J (2021). ZBTB Transcription Factors: Key Regulators of the Development, Differentiation and Effector Function of T Cells. Front Immunol 12, 713294. [PubMed: 34349770]

Cherry TJ, Yang MG, Harmin DA, Tao P, Timms AE, Bauwens M, Allikmets R, Jones EM, Chen R, De Baere E, et al. (2020). Mapping the cis-regulatory architecture of the human retina reveals noncoding genetic variation in disease. Proc Natl Acad Sci U S A 117, 9001–9012. [PubMed: 32265282]

Chirco KR, Chew S, Moore AT, Duncan JL and Lamba DA (2021). Allele-specific gene editing to rescue dominant CRX-associated LCA7 phenotypes in a retinal organoid model. Stem Cell Reports 16, 2690–2702. [PubMed: 34653402]

Clark BS, Stein-O'Brien GL, Shiau F, Cannon GH, Davis-Marcisak E, Sherman T, Santiago CP, Hoang TV, Rajaii F, James-Esposito RE, et al. (2019). Single-Cell RNA-Seq Analysis of Retinal Development Identifies NFI Factors as Regulating Mitotic Exit and Late-Born Cell Specification. Neuron 102, 1111–1126 e1115. [PubMed: 31128945]

Collin J, Queen R, Zerti D, Dorgau B, Hussain R, Coxhead J, Cockell S and Lako M (2019). Deconstructing Retinal Organoids: Single Cell RNA-Seq Reveals the Cellular Components of Human Pluripotent Stem Cell-Derived Retina. Stem Cells 37, 593–598. [PubMed: 30548510]

Corbo JC and Cepko CL (2005). A hybrid photoreceptor expressing both rod and cone genes in a mouse model of enhanced S-cone syndrome. PLoS Genet 1, e11. [PubMed: 16110338]

Cowan CS, Renner M, De Gennaro M, Gross-Scherf B, Goldblum D, Hou Y, Munz M, Rodrigues TM, Krol J, Szikra T, et al. (2020). Cell Types of the Human Retina and Its Organoids at Single-Cell Resolution. Cell 182, 1623–1640 e1634. [PubMed: 32946783]

Cuevas E, Holder DL, Alshehri AH, Treguier J, Lakowski J and Sowden JC (2021). NRL(−/−) gene edited human embryonic stem cells generate rod-deficient retinal organoids enriched in S-cone-like photoreceptors. Stem Cells 39, 414–428. [PubMed: 33400844]

de Martin X, Sodaei R and Santpere G (2021). Mechanisms of Binding Specificity among bHLH Transcription Factors. Int J Mol Sci 22.

Eldred KC, Avelis C, Johnston RJ Jr. and Roberts E (2020). Modeling binary and graded cone cell fate patterning in the mouse retina. PLoS Comput Biol 16, e1007691. [PubMed: 32150546]

Eldred KC, Hadyniak SE, Hussey KA, Brenerman B, Zhang PW, Chamling X, Sluch VM, Welsbie DS, Hattar S, Taylor J, et al. (2018). Thyroid hormone signaling specifies cone subtypes in human retinal organoids. Science 362.

Elliott J, Jolicoeur C, Ramamurthy V and Cayouette M (2008). Ikaros Confers Early Temporal Competence to Mouse Retinal Progenitor Cells. Neuron 60, 26–39. [PubMed: 18940586]

Emerson MM, Surzenko N, Goetz JJ, Trimarchi J and Cepko CL (2013). Otx2 and Onecut1 promote the fates of cone photoreceptors and horizontal cells and repress rod photoreceptors. Dev Cell 26, 59–72. [PubMed: 23867227]

Fenouil R, Cauchy P, Koch F, Descostes N, Cabeza JZ, Innocenti C, Ferrier P, Spicuglia S, Gut M, Gut I, et al. (2012). CpG islands and GC content dictate nucleosome depletion in a transcription-independent manner at mammalian promoters. Genome Res 22, 2399–2408. [PubMed: 23100115]

Finkbeiner C, Ortuno-Lizaran I, Sridhar A, Hooper M, Petter S and Reh TA (2022). Single-cell ATAC-seq of fetal human retina and stem-cell-derived retinal organoids shows changing chromatin landscapes during cell fate acquisition. Cell Reports 38, 110294. [PubMed: 35081356]

Fossat N, Le Greneur C, Beby F, Vincent S, Godement P, Chatelain G and Lamonerie T (2007). A new GFP-tagged line reveals unexpected Otx2 protein localization in retinal photoreceptors. BMC Dev Biol 7, 122. [PubMed: 17980036]

Furukawa T, Morrow EM and Cepko CL (1997). Crx, a novel otx-like homeobox gene, shows photoreceptor-specific expression and regulates photoreceptor differentiation. Cell 91, 531–541. [PubMed: 9390562]

Furukawa T, Morrow EM, Li T, Davis FC and Cepko CL (1999). Retinopathy and attenuated circadian entrainment in Crx-deficient mice. Nat Genet 23, 466–470. [PubMed: 10581037]

Ghinia Tegla MG, Buenaventura DF, Kim DY, Thakurdin C, Gonzalez KC and Emerson MM (2020). OTX2 represses sister cell fate choices in the developing retina to promote photoreceptor specification. Elife 9.

Goodson NB, Kaufman MA, Park KU and Brzezinski JA (2020a). Simultaneous deletion of Prdm1 and Vsx2 enhancers in the retina alters photoreceptor and bipolar cell fate specification, yet differs from deleting both genes. Development 147.

Goodson NB, Park KU, Silver JS, Chiodo VA, Hauswirth WW and Brzezinski J. A. t. (2020b). Prdm1 overexpression causes a photoreceptor fate-shift in nascent, but not mature, bipolar cells. Dev Biol 464, 111–123. [PubMed: 32562755]

Haider NB, Demarco P, Nystuen AM, Huang X, Smith RS, McCall MA, Naggert JK and Nishina PM (2006). The transcription factor Nr2e3 functions in retinal progenitors to suppress cone cell generation. Vis Neurosci 23, 917–929. [PubMed: 17266784]

Hannenhalli S and Kaestner KH (2009). The evolution of Fox genes and their role in development and disease. Nat Rev Genet 10, 233–240. [PubMed: 19274050]

Haverkamp S, Wassle H, Duebel J, Kuner T, Augustine GJ, Feng G and Euler T (2005). The primordial, blue-cone color system of the mouse retina. J Neurosci 25, 5438–5445. [PubMed: 15930394]

Hoshino A, Horvath S, Sridhar A, Chitsazan A and Reh TA (2019). Synchrony and asynchrony between an epigenetic clock and developmental timing. Sci Rep 9, 3770. [PubMed: 30842553]

Hoshino A, Ratnapriya R, Brooks MJ, Chaitankar V, Wilken MS, Zhang C, Starostik MR, Gieser L, La Torre A, Nishio M, et al. (2017). Molecular Anatomy of the Developing Human Retina. Dev Cell 43, 763–779 e764. [PubMed: 29233477]

Hughes AE, Enright JM, Myers CA, Shen SQ and Corbo JC (2017). Cell Type-Specific Epigenomic Analysis Reveals a Uniquely Closed Chromatin Architecture in Mouse Rod Photoreceptors. Sci Rep 7, 43184. [PubMed: 28256534]

Javed A, Mattar P, Cui A and Cayouette M (2021). Ikaros family proteins regulate developmental windows in the mouse retina through convergent and divergent transcriptional programs. BioRxiv.

Javed A, Mattar P, Lu S, Kruczek K, Kloc M, Gonzalez-Cordero A, Bremner R, Ali RR and Cayouette M (2020). Pou2f1 and Pou2f2 cooperate to control the timing of cone photoreceptor production in the developing mouse retina. Development 147.

Jean-Charles N, Buenaventura DF and Emerson MM (2018). Identification and characterization of early photoreceptor cis-regulatory elements and their relation to Onecut1. Neural Dev 13, 26. [PubMed: 30466480]

Jeon CJ, Strettoi E and Masland RH (1998). The major cell populations of the mouse retina. J Neurosci 18, 8936–8946. [PubMed: 9786999]

Jones I, Ng L, Liu H and Forrest D (2007). An Intron Control Region Differentially Regulates Expression of Thyroid Hormone Receptor {beta}2 in the Cochlea, Pituitary, and Cone Photoreceptors. Mol Endocrinol 21, 1108–1119. [PubMed: 17341594]

Jorstad NL, Wilken MS, Todd L, Finkbeiner C, Nakamura P, Radulovich N, Hooper MJ, Chitsazan A, Wilkerson BA, Rieke F, et al. (2020). STAT Signaling Modifies Ascl1 Chromatin Binding and Limits Neural Regeneration from Muller Glia in Adult Mouse Retina. Cell Rep 30, 2195–2208 e2195. [PubMed: 32075759]

Kallman A, Capowski EE, Wang J, Kaushik AM, Jansen AD, Edwards KL, Chen L, Berlinicke CA, Joseph Phillips M, Pierce EA, et al. (2020). Investigating cone photoreceptor development using patient-derived NRL null retinal organoids. Commun Biol 3, 82. [PubMed: 32081919]

Kaufman ML, Goodson NB, Park KU, Schwanke M, Office E, Schneider SR, Abraham J, Hensley A, Jones KL and Brzezinski JA (2021). Initiation of Otx2 expression in the developing mouse retina requires a unique enhancer and either Ascl1 or Neurog2 activity. Development 148.

Kaufman ML, Park KU, Goodson NB, Chew S, Bersie S, Jones KL, Lamba DA and Brzezinski J. A. t. (2019). Transcriptional profiling of murine retinas undergoing semi-synchronous cone photoreceptor differentiation. Dev Biol 453, 155–167. [PubMed: 31163126]

Kim DS, Matsuda T and Cepko CL (2008). A core paired-type and POU homeodomain-containing transcription factor program drives retinal bipolar cell gene expression. J Neurosci 28, 7748–7764. [PubMed: 18667607]

Kim JW, Yang HJ, Oel AP, Brooks MJ, Jia L, Plachetzki DC, Li W, Allison WT and Swaroop A (2016). Recruitment of Rod Photoreceptors from Short-Wavelength-Sensitive Cones during the Evolution of Nocturnal Vision in Mammals. Dev Cell 37, 520–532. [PubMed: 27326930]

Kim S, Lowe A, Dharmat R, Lee S, Owen LA, Wang J, Shakoor A, Li Y, Morgan DJ, Hejazi AA, et al. (2019). Generation, transcriptome profiling, and functional validation of cone-rich human retinal organoids. Proc Natl Acad Sci U S A 116, 10824–10833. [PubMed: 31072937]

Koike C, Nishida A, Ueno S, Saito H, Sanuki R, Sato S, Furukawa A, Aizawa S, Matsuo I, Suzuki N, et al. (2007). Functional roles of Otx2 transcription factor in postnatal mouse retinal development. Molecular and cellular biology 27, 8318–8329. [PubMed: 17908793]

La Vail MM, Rapaport DH and Rakic P (1991). Cytogenesis in the monkey retina. J Comp Neurol 309, 86–114. [PubMed: 1894769]

Lamb TD (2020). Evolution of the genes mediating phototransduction in rod and cone photoreceptors. Prog Retin Eye Res 76, 100823. [PubMed: 31790748]

Lee J, Myers CA, Williams N, Abdelaziz M and Corbo JC (2010). Quantitative fine-tuning of photoreceptor cis-regulatory elements through affinity modulation of transcription factor binding sites. Gene Ther 17, 1390–1399. [PubMed: 20463752]

Liu H, Etter P, Hayes S, Jones I, Nelson B, Hartman B, Forrest D and Reh TA (2008). NeuroD1 Regulates Expression of Thyroid Hormone Receptor 2 and Cone Opsins in the Developing Mouse Retina. J. Neurosci. 28, 749–756. [PubMed: 18199774]

Lonfat N, Wang S, Lee C, Garcia M, Choi J, Park PJ and Cepko C (2021). Cis-regulatory dissection of cone development reveals a broad role for Otx2 and Oc transcription factors. Development 148.

Lu Y, Shiau F, Yi W, Lu S, Wu Q, Pearson JD, Kallman A, Zhong S, Hoang T, Zuo Z, et al. (2020). Single-Cell Analysis of Human Retina Identifies Evolutionarily Conserved and Species-Specific Mechanisms Controlling Development. Dev Cell 53, 473–491 e479. [PubMed: 32386599]

Lyu P, Hoang T, Santiago CP, Thomas ED, Timms AE, Appel H, Gimmen M, Le N, Jiang L, Kim DW, et al. (2021). Gene regulatory networks controlling temporal patterning, neurogenesis, and cell-fate specification in mammalian retina. Cell Rep 37, 109994. [PubMed: 34788628]

Madisen L, Zwingman TA, Sunkin SM, Oh SW, Zariwala HA, Gu H, Ng LL, Palmiter RD, Hawrylycz MJ, Jones AR, et al. (2010). A robust and high-throughput Cre reporting and characterization system for the whole mouse brain. Nat Neurosci 13, 133–140. [PubMed: 20023653]

Maeda T (2016). Regulation of hematopoietic development by ZBTB transcription factors. Int J Hematol 104, 310–323. [PubMed: 27250345]

Mears AJ, Kondo M, Swain PK, Takada Y, Bush RA, Saunders TL, Sieving PA and Swaroop A (2001). Nrl is required for rod photoreceptor development. Nat Genet 29, 447–452. [PubMed: 11694879]

Mills TS, Eliseeva T, Bersie SM, Randazzo G, Nahreini J, Park KU and Brzezinski J. A. t. (2017). Combinatorial regulation of a Blimp1 (Prdm1) enhancer in the mouse retina. PLoS One 12, e0176905. [PubMed: 28829770]

Mori M, Ghyselinck NB, Chambon P and Mark M (2001). Systematic Immunolocalization of Retinoid Receptors in Developing and Adult Mouse Eyes. Invest. Ophthalmol. Vis. Sci. 42, 1312–1318. [PubMed: 11328745]

Morrow EM, Furukawa T, Lee JE and Cepko CL (1999). NeuroD regulates multiple functions in the developing neural retina in rodent. Development 126, 23–36. [PubMed: 9834183]

Muranishi Y, Terada K, Inoue T, Katoh K, Tsujii T, Sanuki R, Kurokawa D, Aizawa S, Tamaki Y and Furukawa T (2011). An essential role for RAX homeoprotein and NOTCH-HES signaling in Otx2 expression in embryonic retinal photoreceptor cell fate determination. J Neurosci 31, 16792–16807. [PubMed: 22090505]

Murphy DP, Hughes AE, Lawrence KA, Myers CA and Corbo JC (2019). Cis-regulatory basis of sister cell type divergence in the vertebrate retina. Elife 8.

Murre C, Bain G, van Dijk MA, Engel I, Furnari BA, Massari ME, Matthews JR, Quong MW, Rivera RR and Stuiver MH (1994). Structure and function of helix-loop-helix proteins. Biochim Biophys Acta 1218, 129–135. [PubMed: 8018712]

Nadal-Nicolas FM, Kunze VP, Ball JM, Peng BT, Krishnan A, Zhou G, Dong L and Li W (2020). True S-cones are concentrated in the ventral mouse retina and wired for color detection in the upper visual field. Elife 9.

Nakano T, Ando S, Takata N, Kawada M, Muguruma K, Sekiguchi K, Saito K, Yonemura S, Eiraku M and Sasai Y (2012). Self-formation of optic cups and storable stratified neural retina from human ESCs. Cell stem cell 10, 771–785. [PubMed: 22704518]

Ng L, Hurley JB, Dierks B, Srinivas M, Salto C, Vennstrom B, Reh TA and Forrest D (2001). A thyroid hormone receptor that is required for the development of green cone photoreceptors. Nat Genet 27, 94–98. [PubMed: 11138006]

Ng L, Lu A, Swaroop A, Sharlin DS, Swaroop A and Forrest D (2011). Two transcription factors can direct three photoreceptor outcomes from rod precursor cells in mouse retinal development. J Neurosci 31, 11118–11125. [PubMed: 21813673]

Nishida A, Furukawa A, Koike C, Tano Y, Aizawa S, Matsuo I and Furukawa T (2003). Otx2 homeobox gene controls retinal photoreceptor cell fate and pineal gland development. Nat Neurosci 6, 1255–1263. [PubMed: 14625556]

Patoori S, Jean-Charles N, Gopal A, Sulaiman S, Gopal S, Wang B, Souferi B and Emerson MM (2020). Cis-regulatory analysis of Onecut1 expression in fate-restricted retinal progenitor cells. Neural Dev 15, 5. [PubMed: 32192535]

Pei Y, Sierra G, Sivapatham R, Swistowski A, Rao MS and Zeng X (2015). A platform for rapid generation of single and multiplexed reporters in human iPSC lines. Sci Rep 5, 9205. [PubMed: 25777362]

Peng GH, Ahmad O, Ahmad F, Liu J and Chen S (2005). The photoreceptor-specific nuclear receptor Nr2e3 interacts with Crx and exerts opposing effects on the transcription of rod versus cone genes. Human molecular genetics 14, 747–764. [PubMed: 15689355]

Pennesi ME, Cho J-H, Yang Z, Wu SH, Zhang J, Wu SM and Tsai M-J (2003). BETA2/NeuroD1 Null Mice: A New Model for Transcription Factor-Dependent Photoreceptor Degeneration. J. Neurosci. 23, 453–461. [PubMed: 12533605]

Perez-Cervantes C, Smith LA, Nadadur RD, Hughes AEO, Wang S, Corbo JC, Cepko C, Lonfat N and Moskowitz IP (2020). Enhancer transcription identifies cis-regulatory elements for photoreceptor cell types. Development 147.

Roberts MR, Hendrickson A, McGuire CR and Reh TA (2005). Retinoid X receptor (gamma) is necessary to establish the S-opsin gradient in cone photoreceptors of the developing mouse retina. Invest Ophthalmol Vis Sci 46, 2897–2904. [PubMed: 16043864]

Roberts MR, Srinivas M, Forrest D, Morreale de Escobar G and Reh TA (2006). Making the gradient: thyroid hormone regulates cone opsin expression in the developing mouse retina. Proc Natl Acad Sci U S A 103, 6218–6223. [PubMed: 16606843]

Samuel A, Housset M, Fant B and Lamonerie T (2014). Otx2 ChIP-seq reveals unique and redundant functions in the mature mouse retina. PLoS One 9, e89110. [PubMed: 24558479]

Sapkota D, Chintala H, Wu F, Fliesler SJ, Hu Z and Mu X (2014). Onecut1 and Onecut2 redundantly regulate early retinal cell fates during development. Proc Natl Acad Sci U S A 111, E4086–4095. [PubMed: 25228773]

Sato S, Inoue T, Terada K, Matsuo I, Aizawa S, Tano Y, Fujikado T and Furukawa T (2007). Dkk3-Cre BAC transgenic mouse line: a tool for highly efficient gene deletion in retinal progenitor cells. Genesis 45, 502–507. [PubMed: 17661397]

Schick E, McCaffery SD, Keblish EE, Thakurdin C and Emerson MM (2019). Lineage tracing analysis of cone photoreceptor associated cis-regulatory elements in the developing chicken retina. Sci Rep 9, 9358. [PubMed: 31249345]

Schneider CA, Rasband WS and Eliceiri KW (2012). NIH Image to ImageJ: 25 years of image analysis. Nature methods 9, 671–675. [PubMed: 22930834]

Sjoberg M, Vennstrom B and Forrest D (1992). Thyroid hormone receptors in chick retinal development: differential expression of mRNAs for alpha and N-terminal variant beta receptors. Development 114, 39–47. [PubMed: 1576965]

Skinner MK, Rawls A, Wilson-Rawls J and Roalson EH (2010). Basic helix-loop-helix transcription factor gene family phylogenetics and nomenclature. Differentiation 80, 1–8. [PubMed: 20219281]

Souferi B and Emerson MM (2019). Quantitative analysis of the ThrbCRM1-centered gene regulatory network. Biol Open 8.

Sridhar A, Hoshino A, Finkbeiner CR, Chitsazan A, Dai L, Haugan AK, Eschenbacher KM, Jackson DL, Trapnell C, Bermingham-McDonogh O, et al. (2020). Single-Cell Transcriptomic Comparison of Human Fetal Retina, hPSC-Derived Retinal Organoids, and Long-Term Retinal Cultures. Cell Rep 30, 1644–1659 e1644. [PubMed: 32023475]

Swaroop A, Kim D and Forrest D (2010). Transcriptional regulation of photoreceptor development and homeostasis in the mammalian retina. Nature reviews. Neuroscience 11, 563–576. [PubMed: 20648062]

Welby E, Lakowski J, Di Foggia V, Budinger D, Gonzalez-Cordero A, Lun ATL, Epstein M, Patel A, Cuevas E, Kruczek K, et al. (2017). Isolation and Comparative Transcriptome Analysis of Human Fetal and iPSC-Derived Cone Photoreceptor Cells. Stem Cell Reports 9, 1898–1915. [PubMed: 29153988]

Wilken MS, Brzezinski JA, La Torre A, Siebenthall K, Thurman R, Sabo P, Sandstrom RS, Vierstra J, Canfield TK, Hansen RS, et al. (2015). DNase I hypersensitivity analysis of the mouse brain and retina identifies region-specific regulatory elements. Epigenetics Chromatin 8, 8. [PubMed: 25972927]

Wu J, Xu J, Liu B, Yao G, Wang P, Lin Z, Huang B, Wang X, Li T, Shi S, et al. (2018). Chromatin analysis in human early development reveals epigenetic transition during ZGA. Nature 557, 256–260. [PubMed: 29720659]

Xiang M (2013). Intrinsic control of mammalian retinogenesis. Cellular and molecular life sciences : CMLS 70, 2519–2532. [PubMed: 23064704]

Yamamoto H, Kon T, Omori Y and Furukawa T (2020). Functional and Evolutionary Diversification of Otx2 and Crx in Vertebrate Retinal Photoreceptor and Bipolar Cell Development. Cell Rep 30, 658–671 e655. [PubMed: 31968244]

Zhong X, Gutierrez C, Xue T, Hampton C, Vergara MN, Cao LH, Peters A, Park TS, Zambidis ET, Meyer JS, et al. (2014). Generation of three-dimensional retinal tissue with functional photoreceptors from human iPSCs. Nature communications 5, 4047.

Highlights:

- An intronic enhancer within *Pde6c* drives expression in developing cones.
- Transgenic retinal organoid systems show that the enhancer is active in human cones.
- The *Pde6c* enhancer is activated by cells deciding between rod and cone fates.
- The enhancer likely has five or more essential transcription factor binding regions.
- Moderate conservation suggests flexibility of enhancer function between species.

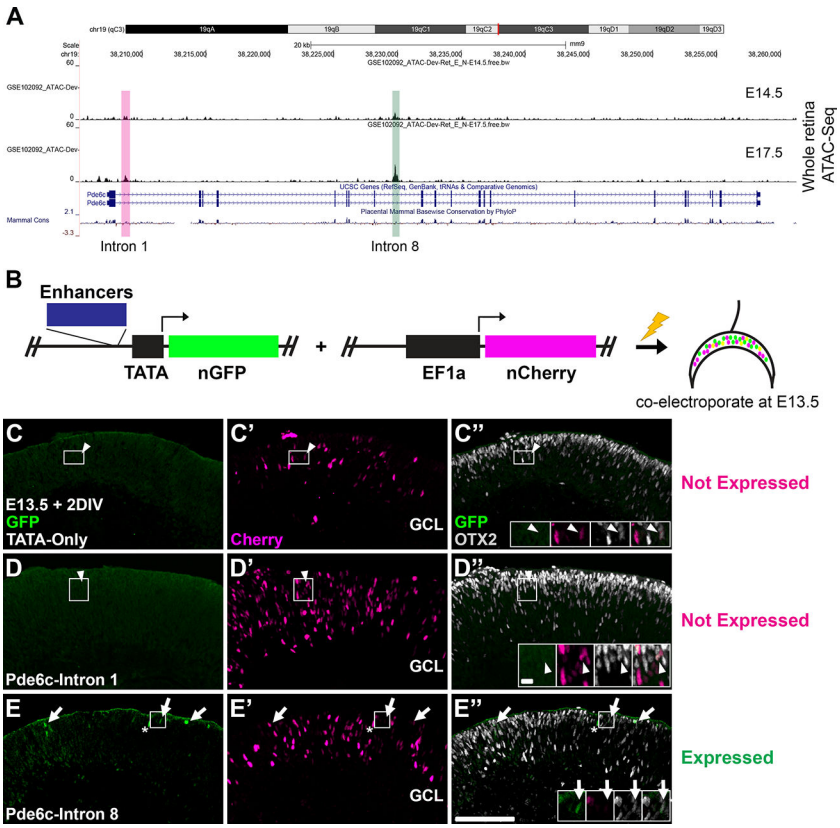

Figure 1.

Identification of an enhancer within the mouse *Pde6c* gene. **(A)** UCSC Genome Browser view of mouse chromosome 19 (*mm9* assembly) showing whole retina ATAC-sequencing data from E14.5 and E17.5 time points (see Aldiri et al, 2017). The structure of the *Pde6c* gene is shown along with mammalian conservation. The ATAC-seq peaks within introns 1 and 8 are highlighted. These intronic sequences have modest conservation compared to the exons. **(B)** Enhancer screening strategy. Potential enhancer sequences are cloned upstream of a minimal TATA promoter to drive nuclear-localized (n) GFP expression. The positive control plasmid uses the ubiquitous *EF1a* promoter to drive nCherry in all electroporated cells. E13.5 retinal explants are co-electroporated with a 1:1 mixture of plasmids and cultured for 2 days *in vitro* (DIV). **(C-E")** Histology of retinal explants stained with antibodies against GFP, RFP (Cherry), and OTX2. **(C-C")** Negative control plasmids lacking any enhancer elements have little to no GFP expression. Arrowheads mark Cherry+ cells that co-express OTX2, but lack GFP. **(D-D")** The intron 1 element does not show GFP activity, though Cherry+ cells are abundant. Arrowheads mark Cherry+/OTX2+ cells that lack GFP. **(E-E")** The intron 8 element shows GFP expression in the outer-most aspect of the retinal explant, consistent with photoreceptor identity. Just a small fraction of the electroporated cells is GFP+. Arrows mark examples of GFP+ cells that co-express the photoreceptor marker OTX2. Asterisks mark a rare GFP+ cell that lacks OTX2 expression. Note that elevated background in the GFP channel (green) is occasionally observed when the number of GFP+ cells is low. Only the bright GFP+ nuclei are considered positive. Scale bar for panels is 100 μm and 10 μm for insets. GCL, ganglion cell layer.

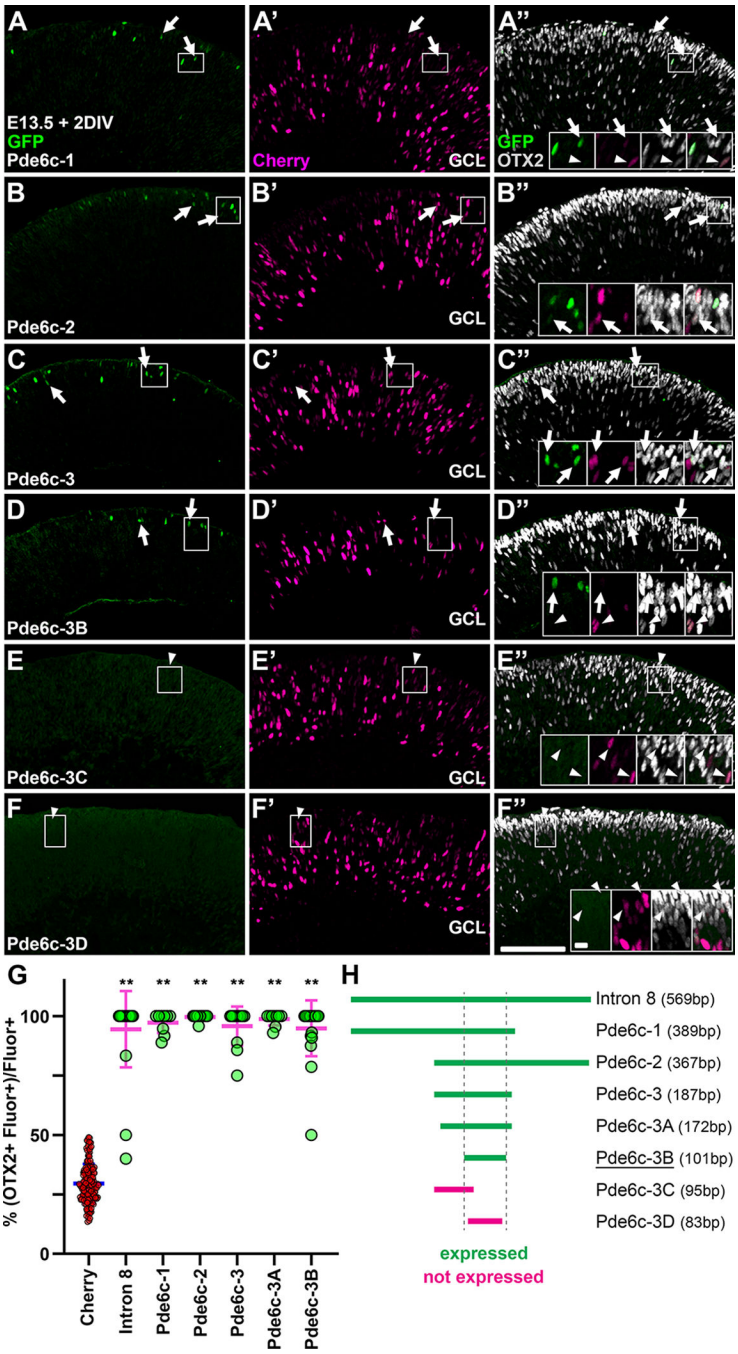

Figure 2.

Multiple sub-elements of the *Pde6c* intron 8 sequence are expressed by OTX2+ cells in mice. **(A-F")** E13.5 explants co-electroporated with enhancer sub-element and nCherry control plasmids and cultured for 2 DIV. Sections are stained for GFP, RFP (Cherry), and OTX2. **(A-A")** Intron 8 sub-element 1 (Pde6c-1) drives GFP expression in the outer part of the retina. Arrows show GFP+ cells that co-express OTX2. Arrowheads mark cells that co-express only Cherry and OTX2. **(B-D")** Pde6c-2 (B), Pde6c-3 (C) and Pde6c-3B (D) elements each drive GFP expression in the outer-most aspect of the retina. Arrows mark

GFP+ cells that co-express OTX2. Arrowheads mark Cherry+/OTX2+ cells that lack GFP. For each sub-element (1, 2, 3, and 3B), only a small fraction of the electroporated cell population co-expresses GFP. **(E-F")** Pde6c-3C (E) and Pde6c-3D (F) elements fail to drive GFP expression. Arrowheads mark Cherry+ cells that co-express OTX2, but lack GFP. Scale bar for panels is 100 μm and 10 μm for insets. GCL, ganglion cell layer. **(G)** Plot showing the percentage of GFP or Cherry positive cells that co-express OTX2. Each circle represents a quantified 200X image. The bars show the mean and standard deviation. The biological N (number of explants) and technical n (images) for each sample is: Cherry (N=64, n=170), intron 8 (N=11, n=23), Pde6c-1 (N=6, n=9), Pde6c-2 (N=6, n=11), Pde6c-3 (N=8, n=12), Pde6c-3A (N=5, n=9), Pde6c-3B (N=8, n=21). Kruskal-Wallis non-parametric ANOVA shows a significant difference ($P < 0.001$) between the groups. Dunn's multiple comparison tests between each condition show that all GFP expressing sub-elements are significantly different than Cherry control (**, $P < 0.001$). However, there are no significant differences between any active enhancer pairs. Some of the variability is due to the relatively low number of GFP+ cells seen in 200X images. **(H)** Graphic showing the intron 8 parental enhancer element and its sub-elements at scale. Sub-elements Pde6c-3C and Pde6c-3D are not expressed (magenta). The dotted lines show the smallest element (Pde6c-3B) that retains GFP expression.

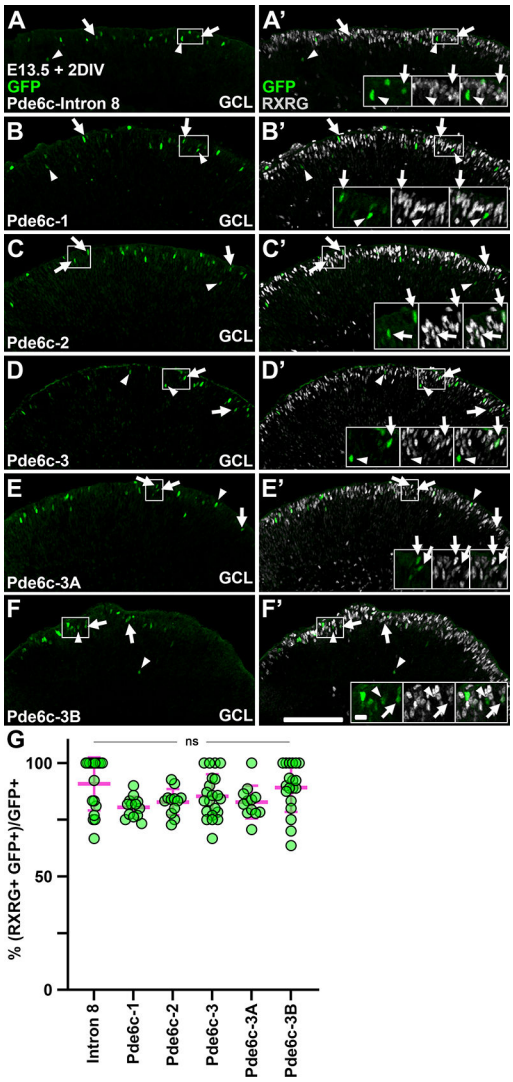

Figure 3.

Enhancer labeled cells co-express the cone marker RXRG in mice. **(A-F')** E13.5 explants electroporated with enhancer plasmids and cultured for 2 DIV. Sections are stained for GFP and RXRG. **(A-A')** The parental intron 8 enhancer drives GFP expression in the outer-most aspect of the retina. The majority of these cells co-express RXRG (arrows). Arrowheads mark examples of GFP+ cells that lack RXRG co-expression. **(B-F')** Pde6c-1 (B), Pde6c-2 (C), Pde6c-3 (D), Pde6c-3A (E), and Pde6c-3B (F) sub-element constructs show GFP activity in the outer aspect of the retina, similar to the intron 8 construct. The majority of GFP+ cells co-express RXRG (arrows) while arrowheads mark examples of GFP+ cells that lack RXRG co-expression. Scale bar for panels is 100 μm and 10 μm for insets. GCL, ganglion cell layer. **(G)** Plot showing the percentage of GFP positive cells that co-express RXRG. Each circle represents a quantified 200X image. The bars show the mean and standard deviation. The biological N (number of explants) and technical n (images) for each sample is: intron 8 (N=11, n=18), Pde6c-1 (N=6, n=13), Pde6c-2 (N=6, n=12), Pde6c-3 (N=6, n=21), Pde6c-3A (N=5, n=12), Pde6c-3B (N=9, n=19). Kruskal-Wallis non-

parametric ANOVA shows a significant difference (P =0.021) between the groups. However, Dunn's multiple comparison tests between conditions do not show a significant difference between any enhancer pair. ns, not significant. Some of the variability is due to the relatively low number of GFP+ cells seen in 200X images.

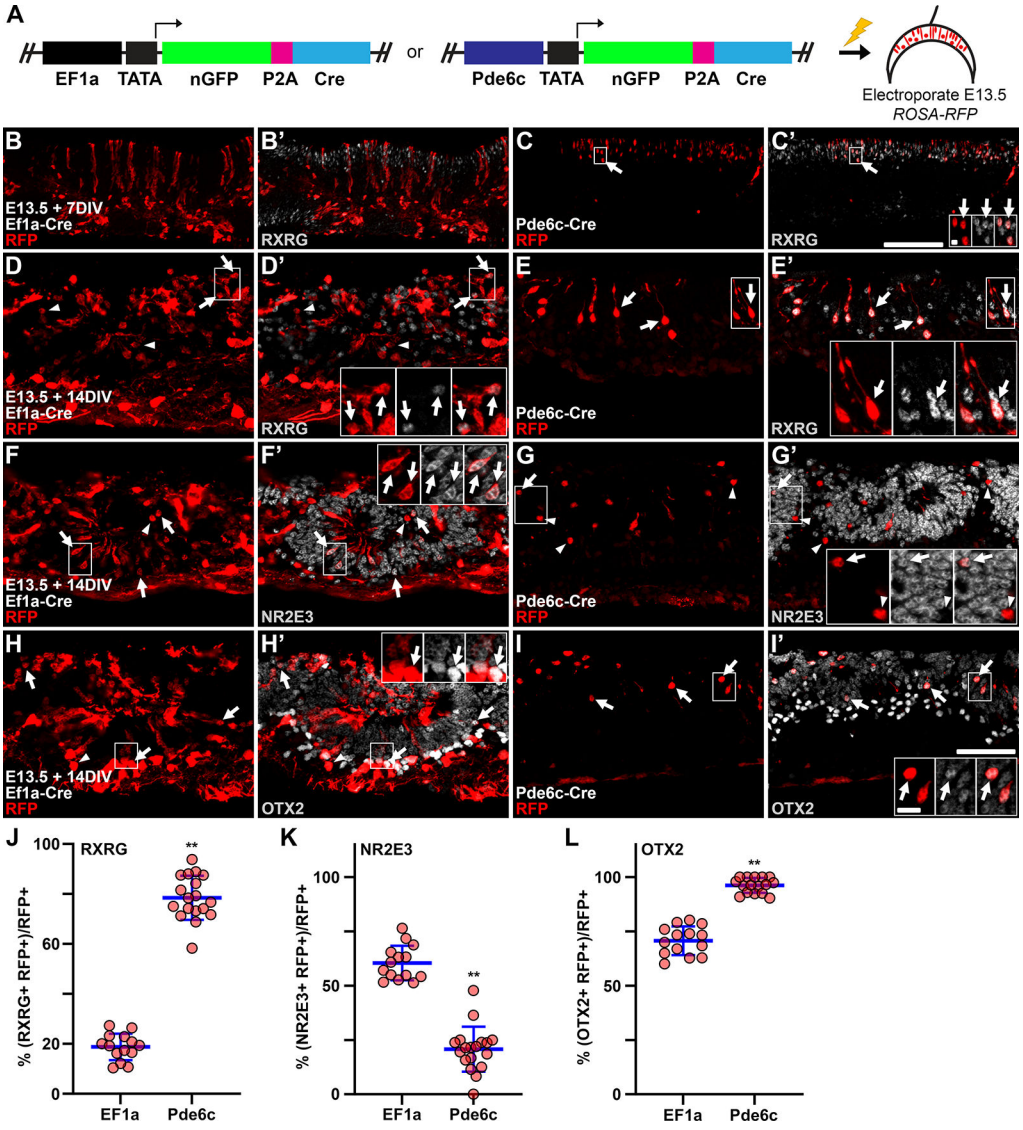

Figure 4.

The *Pde6c* enhancer lineage primarily comprises cones in mice. **(A)** Schematic of lineage tracing experiment. A ubiquitously expressed EF1a-GFP-Cre plasmid is used to trace the lineage of all electroporated cells. The Pde6c-intron 8-GFP-Cre plasmid is used to trace cells that activate the *Pde6c* enhancer. Plasmids were electroporated into E13.5 *ROSA-RFP* retinal explants and cultured for 7 or 14 DIV. Recombined cells permanently express cytoplasmic tdTomato (RFP). **(B-C')** *EF1a* (B) and *Pde6c* (C) lineages after 7 DIV. **(B-B')** RFP+ lineage traced cells in the *EF1a* condition show morphologies consistent with photoreceptors (thin/short), interneurons (round/large), and progenitors (thin/elongated). A small fraction co-expresses RXRG. **(C-C')** The morphology of RFP+ cells in *Pde6c* lineage traced conditions are overwhelmingly photoreceptor-like. Nearly all of the RFP+ cells co-express RXRG (arrows). Scale bar for panels B-C' is 100 μm and 5 μm for insets. **(D-I')** *EF1a* (D, F, H) and *Pde6c* (E, G, I) lineages after 14 DIV. Sections are stained for RFP and either RXRG (D-E'), NR2E3 (F-G'), or OTX2 (H-I'). Rosettes are

common after 14 DIV. **(D-E')** Control lineage tracing (D) shows abundant RFP+ cells throughout electroporated regions. These cells primarily have interneuron and photoreceptor morphologies. Arrowheads mark examples of cells with photoreceptor morphology that lack RXRG staining (*i.e.*, rods). Arrows mark examples of RFP+/RXRG+ cells (*i.e.*, cones). *Pde6c* lineage traced cells (E) are sparse and show photoreceptor morphology with a prominent soma and thin apical processes. Most of these RFP+ cells co-express RXRG (arrows). **(F-G')** *EF1a* lineage traced retinas (F) have numerous examples of RFP+/NR2E3+ rods. In contrast, relatively few RFP+ cells in the *Pde6c* lineage (G) co-express NR2E3. Arrows mark RFP+/NR2E3+ cells and arrowheads denote single-labeled cells. **(H-I')** The majority of RFP+ cells in *EF1a* (H) and *Pde6c* (I) lineage tracings co-express OTX2. In the *EF1a* lineage, there are examples of intense and dim OTX2 overlap (arrows), indicative of bipolar cell and photoreceptor identities, respectively. Arrowheads mark RFP+ cells that lack OTX2. In the *Pde6c* lineage, nearly all of the RFP+ cells co-express OTX2 (arrows). Scale bar for panels D-I is 50 μm and 10 μm for insets. Due to the presence of rosettes, orienting images with the outer retina towards the top was imprecise. **(J-L)** Plots showing the percentage of RFP positive cells that co-express RXRG (J), NR2E3 (K), and OTX2 (L). Each circle represents a quantified 200X image. The bars show the mean and standard deviation. The biological N (number of explants) and technical n (images) for each sample is: EF1a (N=4, n=14 for NR2E3, RXRG, and OTX2) and Pde6c (N=4, n=18 for NR2E3, RXRG and n=16 for OTX2). Mann-Whitney two-tailed non-parametric tests show significant differences between *EF1a* and *Pde6c* for RXRG (**, $P < 0.0001$), NR2E3 (**, $P < 0.0001$) and OTX2 (**, $P < 0.0001$) overlap.

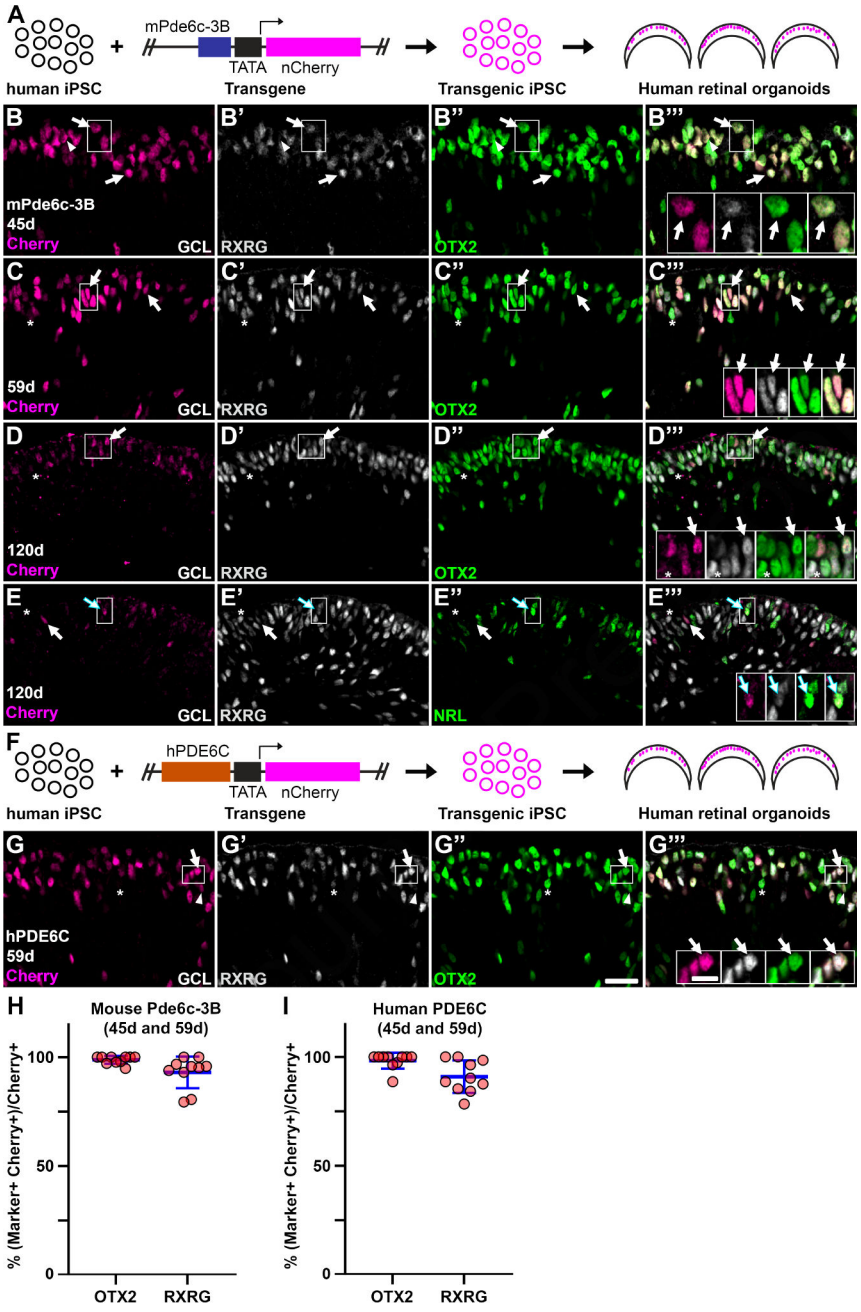

Figure 5.

The *Pde6c* enhancer marks developing cones in human retinal organoids. **(A)** Schematic of how transgenic iPSCs were made (see Fig S6 for more details). The mouse (m) *Pde6c* intron 8 element was cloned into a vector driving nCherry. Cassette exchange in iPSCs resulted in the integration of the transgene (magenta outline). Transgenic iPSCs were then differentiated into 3D human retinal organoids. **(B-E"')** Organoids derived from mPde6c-3B-nCherry transgenic iPSCs stained for RFP (Cherry) and photoreceptor markers. **(B-B"')** At 45 days (d) of culture, transgenic organoids have a large number of Cherry+ cells in the outer aspect of the retina. This is similar to the RXRG (cone) and OTX2 (photoreceptor)

patterns. Arrows mark examples of Cherry+/RXRG+/OTX2+ cells. Arrowheads mark a Cherry+ cell that co-expresses OTX2, but not RXRG. Nearly all of the RXRG+/OTX2+ cells (cones) co-express Cherry. **(C-C”’)** At 59d, transgenic organoids have a similar number of Cherry+ cells and most co-express RXRG and OTX2 (arrows). The asterisk marks a rare example of a RXRG+/OTX2+ cone that lacks Cherry expression. **(D-E”’)** 120d organoids stained with photoreceptor markers. At 120d, most of the cones have formed and rods are being generated in greater numbers. The number of Cherry+ cells is reduced and expression is weaker than at earlier time points. **(D-D”’)** A few examples of Cherry+/RXRG+/OTX2+ cells (arrows) are still seen at 120d. However, most of the RXRG+/OTX2+ cones lack appreciable Cherry signal (asterisks). **(E-E”’)** A small number of Cherry+ cells co-express the rod marker NRL (blue outlined arrows). Some of these Cherry+/NRL+ cells co-express a modest amount of RXRG. White arrows mark examples of cells that co-express Cherry and RXRG. Asterisks mark examples of RXRG+ cells that lack Cherry signal. **(F)** Schematic showing how transgenic iPSCs were made. In this case, the human (h) sequence homologous to mouse intron 8 (*hPDE6C*) was used to drive nCherry and make transgenic iPSCs (magenta outline). **(G-G”’)** Human retinal organoids made from hPDE6C-Cherry iPSCs after 59d of growth stained for RFP (Cherry), RXRG, and OTX2. There are abundant Cherry+ cells located primarily in the outer aspect of the retina. The Cherry+ cells frequently overlap with RXRG and OTX2 (arrows). Arrowheads mark rare examples of Cherry+/OTX2+ cells that do not express RXRG. The asterisks mark rare examples of RXRG+/OTX2+ cones that lack Cherry signal. Scale bar for panels is 25 μm and 10 μm for insets. GCL, ganglion cell layer. **(H-I)** Plots showing the percentage of Cherry positive cells that co-express OTX2 and RXRG in the mPde6c (H) and hPDE6C (I) transgenic organoids. Each circle represents a quantified 400X image. The bars show the mean and standard deviation. The biological N (number of organoids) and technical n (images) for each sample is: 45d mPde6c (N=5, n=5), 45d hPDE6C (N=5, n=5), 59d mPde6c (N=5, n=5), and 59d hPDE6C (N=5, n=5). The plots show combined data from 45d and 59d. Kruskal-Wallis one-way ANOVA and Dunn’s multiple comparisons tests did not reveal a significant difference in marker overlap between 45d and 59d time points. No significant differences in marker overlaps between mouse and human enhancers are seen.

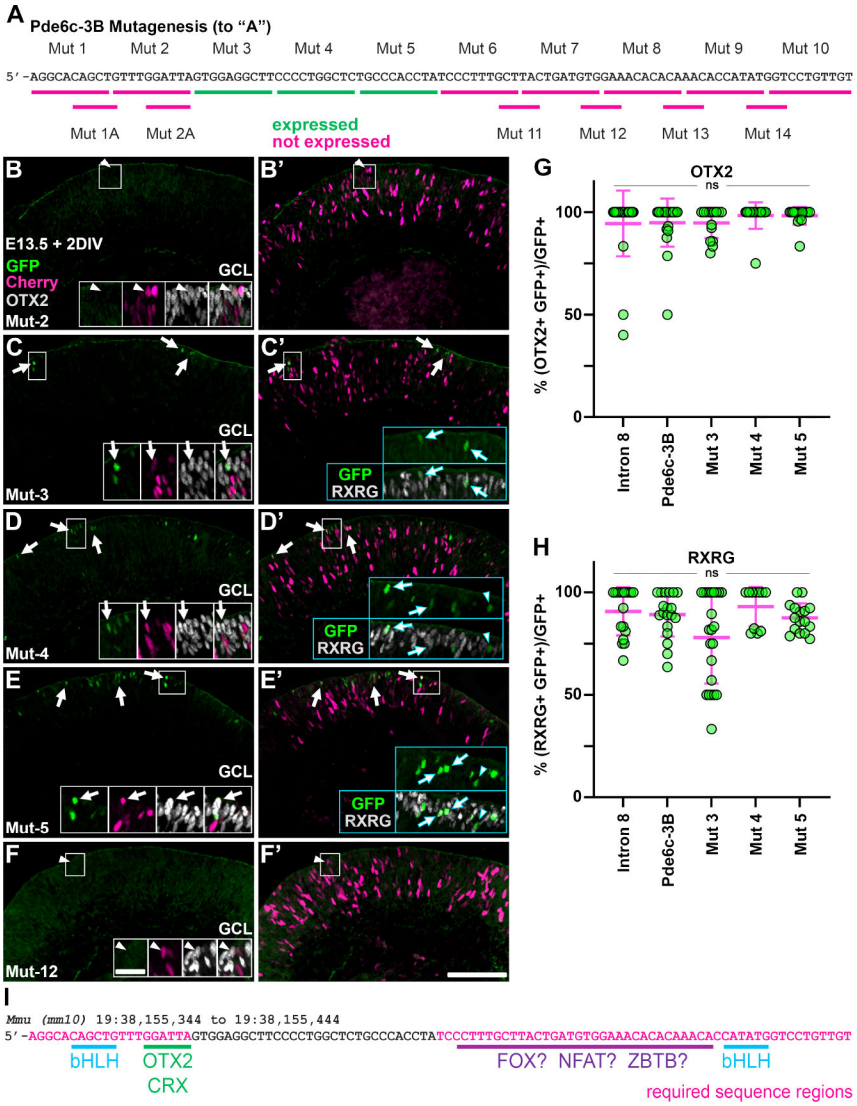

Figure 6.

Systematic tiled mutagenesis reveals necessary sequences in the Pde6c-3B enhancer. **(A)** Schematic of the *Pde6c-3B* sequence showing the location of mutated (Mut) bases. Sequences were mutated to adenine ("A") to maintain the same overall length. Mutant constructs that retain expression are labeled in green and those that lack activity are in magenta. **(B-F')** E13.5 mouse retinal explants co-electroporated with EF1a-nCherry control and Mut plasmids and cultured for 2 DIV. Sections are stained for GFP, RFP (Cherry), and OTX2 (white insets). Different sections are stained for GFP and RXRG (blue insets). **(B-B')** Mut 2 electroporated retinas lack GFP activity. Arrowheads mark examples of Cherry+ cells that co-express OTX2. **(C-E')** Mut 3 (C), Mut 4 (D), and Mut 5 (E) constructs drive GFP activity in the outer-most retina. Mut 3 electroporated retinas (C) appeared to have fewer GFP+ cells than Mut 4 (D) and Mut 5 (E) conditions. In all three of these mutants, GFP+ cells extensively co-express OTX2 (white arrows, white insets). Shown in blue insets, GFP+ cells frequently co-express RXRG (blue arrows). Blue outlined arrowheads mark examples of GFP+ cells that lack RXRG. **(F-F')** Mut 12 electroporated retinas lack GFP expression.

Arrowheads mark Cherry+ cells that co-express OTX2. Scale bar for panels is 100 μm and 25 μm for insets. GCL, ganglion cell layer. **(G-H)** Plots showing the percentage of GFP positive cells that co-express OTX2 (G) and RXRG (H). Each circle represents a quantified 200X image. The bars show the mean and standard deviation. The biological N (number of explants) and technical n (images) for each sample is: Intron 8 (N=11, n=23 OTX2, n=18 RXRG), Pde6c-3B (N=8, n=21 OTX2, n=19 RXRG), Mut 3 (N=7, n=15 OTX2, n=23 RXRG), Mut 4 (N=5, n=15 OTX2, n=11 RXRG), and Mut 5 (N=5, n=16 OTX2 and RXRG). Counts from intron 8 and Pde6c-3B are from figures 2 and 3. Kruskal-Wallis one-way ANOVA with Dunn's multiple comparison tests between each condition does not show a significant difference between any enhancer pair in percentage overlap with OTX2 or RXRG. Some of the variability, especially for Mut 3, is due to the relatively low number of GFP+ cells seen in 200X images. ns, not significant. **(I)** Schematic showing necessary (magenta) and dispensable (black) sequences in the Pde6c-3B enhancer. JASPAR 2022 predictions of potential transcription factor binding sites. There are strong predictions for two E-boxes (bHLH factor binding) and an OTX2/CRX site. The larger region in purple may bind FOX, NFAT, and/or ZBTB family transcription factors.

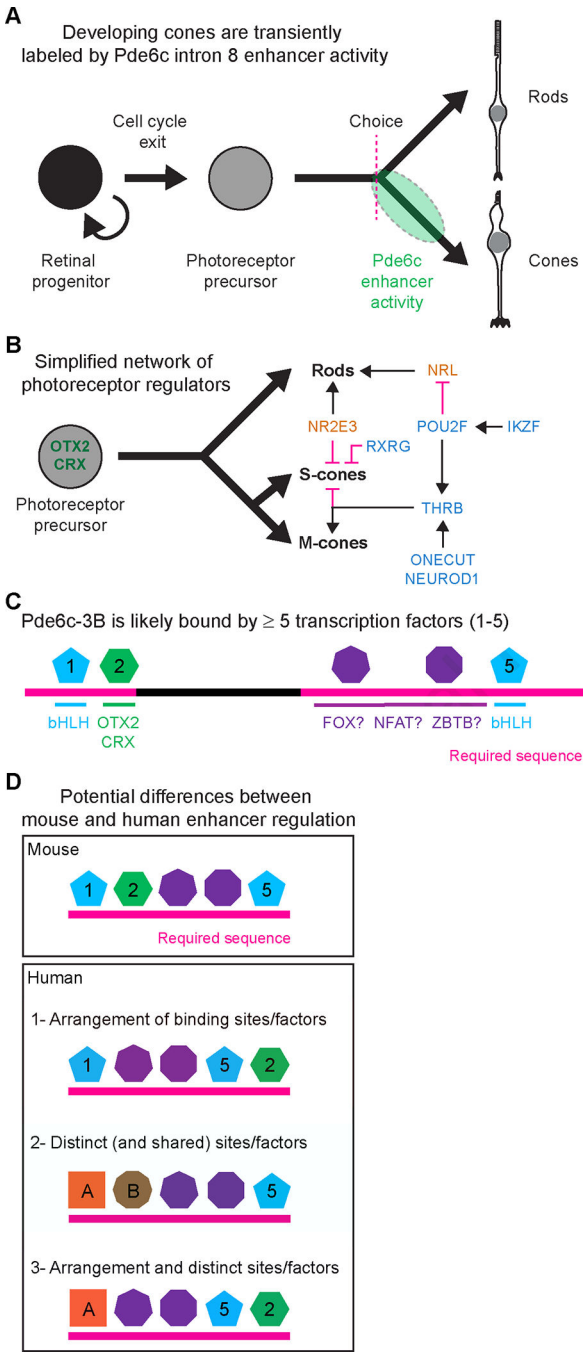

Figure 7.

Model of *Pde6c* enhancer expression and regulation. **(A)** As retinal progenitor cells permanently exit the cell cycle, a large fraction becomes photoreceptor precursors that acquire the potential to adopt rod and cone photoreceptor identity. Transient *Pde6c* enhancer activity (green) is seen primarily in cones, but also in a small population of cells that acquire rod fate. This suggests that the *Pde6c* enhancer becomes active when photoreceptor fate choice decisions (dotted magenta line) are being made. **(B)** A simplified schematic showing transcription factors that regulate photoreceptor development. Transcription factors

are colored by their primary expression patterns or roles: pan-photoreceptor (green), rod (brown), and cone (blue). Precursors express OTX2 and CRX (green), which are necessary for photoreceptor formation and gene expression. NRL and NR2E3 promote (black arrows) rods while inhibiting (magenta lines) S-cones. RXRG is made by cones and inhibits S-opsin expression. NEUROD1, POU2F, and ONECUT transcription factors promote THRB expression to promote M-cones. THRB also inhibits S-opsin expression, while POU2F inhibits NRL and rod fate. IKZF factors appear to promote POU2F transcription factor expression. NEUROD1, POU2F, IKZF, and ONECUT factor expression patterns are complex and are also present upstream of photoreceptor fate decisions. **(C)** The mouse *Pde6c-3B* element likely contains five or more transcription factor binding sites in the required sequence region (magenta). Potential transcription factors (polygons) bound to these sites are numbered and colored by type. It is possible that each potential site (1–5) is bound by a different transcription factor. Alternatively, the same transcription factor may bind in multiple locations, such as for bHLH factors (sites 1 & 5) or for those predicted to be bound by FOX, NFAT, or ZBTB factors (sites 3 & 4). Whether specific transcription factors are necessary or can act redundantly with related factors is unknown. **(D)** Models explaining how *Pde6c* enhancers are regulated differently between mouse and human. The mouse *Pde6c-3B* required sequence (magenta) is shown with 5 potential transcription factors bound, as in panel C. In the first scenario, the same transcription factors used in mice regulate the human enhancer, but they are arranged in a different order. This could also include differences in spacing or the number of binding sites for each factor. In the second scenario, there are species-specific differences in the transcription factors that bind the enhancer. In this example, there are both distinct (A & B) and shared (3–5) factors bound to the human enhancer. The final scenario is a combination of the first two, such that there are some transcription factor utilization differences along with changes in the arrangement of binding sites. The sequences required for human enhancer activity remain to be determined.